JGR Atmospheres

RESEARCH ARTICLE
10.1029/2020JD033788

Special Section:
Atmospheric Rivers: Intersection of Weather and Climate

Antarctic Atmospheric River Climatology and Precipitation Impacts

Jonathan D. Wille[1], Vincent Favier[1], Irina V. Gorodetskaya[2], Cécile Agosta[3], Christoph Kittel[4], Jai Chowdhry Beeman[1], Nicolas C. Jourdain[1], Jan T. M. Lenaerts[5], and Francis Codron[6]

[1]Institut des Géosciences de l'Environnement, CNRS/UGA/IRD/G-INP, Saint Martin d'Hères, France, [2]Department of Physics, CESAM – Centre for Environmental and Marine Studies, University of Aveiro, Aveiro, Portugal, [3]LSCE – Laboratoire des Sciences du Climat et l'Environnement, Gif-sur-Yvette, France, [4]Laboratory of Climatology, Department of Geography, University of Liège, Liège, Belgium, [5]Department of Atmospheric and Oceanic Sciences, University of Colorado, Boulder, CO, USA, [6]LOCEAN, Université Pierre and Marie Curie, Paris, France

Abstract The Antarctic ice sheet (AIS) is sensitive to short-term extreme meteorological events that can leave long-term impacts on the continent's surface mass balance (SMB). We investigate the impacts of atmospheric rivers (ARs) on the AIS precipitation budget using an AR detection algorithm and a regional climate model (Modèle Atmosphérique Régional) from 1980 to 2018. While ARs and their associated extreme vapor transport are relatively rare events over Antarctic coastal regions (~3 days per year), they have a significant impact on the precipitation climatology. ARs are responsible for at least 10% of total accumulated snowfall across East Antarctica (localized areas reaching 20%) and a majority of extreme precipitation events. Trends in AR annual frequency since 1980 are observed across parts of AIS, most notably an increasing trend in Dronning Maud Land; however, interannual variability in AR frequency is much larger. This AR behavior appears to drive a significant portion of annual snowfall trends across East Antarctica, while controlling the interannual variability of precipitation across most of the AIS. AR landfalls are most likely when the circumpolar jet is highly amplified during blocking conditions in the Southern Ocean. There is a fingerprint of the Southern Annular Mode (SAM) on AR variability in West Antarctica with SAM+ (SAM−) favoring increased AR frequency in the Antarctic Peninsula (Amundsen-Ross Sea coastline). Given the relatively large influence ARs have on precipitation across the continent, it is advantageous for future studies of moisture transport to Antarctica to consider an AR framework especially when considering future SMB changes.

Plain Language Summary The Antarctic continent, like many deserts in the world, receives a large percentage of its yearly precipitation from just a few intense precipitation events. Atmospheric rivers (ARs), narrow corridors of intense moisture transporting moisture from low to high latitudes, are commonly associated with heavy rain and snowfall in the midlatitudes like the west coasts of North/South America and Europe. In Antarctica, ARs are rarer with most near-coastal regions in Antarctica experiencing AR conditions a few days per year but still have a major influence on the surface mass balance of the ice sheet. ARs are responsible for 10%–20% of the total snowfall across East Antarctica. Although a modest percentage, this contribution to the snowfall budget is the component that has been driving parts of the positive annual snowfall trends in Dronning Maud and negative trends in Wilkes Land. Also, ARs control the year-to-year variability of precipitation across most of the ice sheet. Given the link between ARs and snowfall accumulation trends, increased future AR activity would result in higher snowfall accumulation on the Antarctic continent and possibly offset some sea-level rise from dynamic ice loss, but this must be considered in balance with increased melting frequency already documented with ARs.

Key Points:

- Atmospheric rivers in Antarctica are rare events but are a key contributor to the ice sheet's surface mass balance
- Their impact on precipitation is most pronounced in East Antarctica where they are responsible for a majority of extreme precipitation events
- Atmospheric rivers are contributing to modern snowfall trends and controlling overall precipitation variability across Antarctica

Supporting Information:

Supporting Information may be found in the online version of this article.

Correspondence to:

J. D. Wille,
jonathan.wille@univ-grenoble-alpes.fr

Citation:

Wille, J. D., Favier, V., Gorodetskaya, I. V., Agosta, C., Kittel, C., Beeman, J. C., et al. (2021). Antarctic atmospheric river climatology and precipitation impacts. *Journal of Geophysical Research: Atmospheres*, *126*, e2020JD033788. https://doi.org/10.1029/2020JD033788

Received 31 AUG 2020
Accepted 20 MAR 2021

1. Introduction

The Antarctic ice sheet (AIS) is classified as a polar desert where, similar to other deserts around the world, the annual precipitation is dependent on a few episodic precipitation events. Recent research has highlighted that certain regions of the AIS receive 40%–60% of their total annual precipitation from the largest 10% of daily precipitation events (Turner et al., 2019). There is a high coast-inland snowfall gradient, as most

snowfall that falls in the Antarctic is the result of cyclonic activity advecting marine air masses toward the coastline (Bromwich, 1988; Bromwich et al., 2004; Gorodetskaya et al., 2013, 2015; Grieger et al., 2016; Jullien et al., 2020; Schlosser et al., 2010; Souverijns et al., 2018). Meanwhile, a persistent inland polar anticyclone and the steep slope of the high Antarctic plateau prevents these marine air masses from traveling far inland due to cyclone decay from topographically induced vorticity compression (Agosta, Amory, et al., 2019; Bromwich, 1988; Hobbs, 1915; Kittel et al., 2018). The most common precipitation type for the interior of Antarctica is clear-sky precipitation in the form of very light snow or diamond dust induced by strong radiative cooling (Bromwich, 1988; King & Turner, 2007; Picard et al., 2019; Stenni et al., 2016). Marine air intrusions, although rare, can penetrate far into the Antarctic continent, delivering quick yet relatively intense snowfall. These features are often responsible for the extreme precipitation events (EPEs) across and slightly inland of the Antarctic coastline (Turner et al., 2019). Intrusions of maritime air into the Antarctic interior are frequently the result of large blocking ridges in the Southern Ocean directing air masses from subtropical and midlatitude origin toward the Antarctic continent (Hirasawa et al., 2013; Kurita et al., 2016; Massom et al., 2004; Naithani et al., 2002; Schlosser et al., 2010). Some studies have connected these blocking-related moist air intrusions to atmospheric rivers (ARs) that caused large localized snowfall and melting events (Bozkurt et al., 2018; Gorodetskaya et al., 2014; Kurita et al., 2016; Wille et al., 2019). However, the link between ARs and Antarctic-wide precipitation climatology and surface mass balance (SMB) has not been described yet.

An atmospheric river as defined in the American Meteorological Society Glossary of Meteorology is "a long, narrow, and transient corridor of strong horizontal water vapor transport that is typically associated with a low-level jet stream ahead of the cold front of an extratropical cyclone." ARs often exhibit a moist-stable vertical stratification and produce heavy precipitation when the air parcels are orographically lifted upon landfall or isentropically lifted within the cyclone's warm conveyor belt (Neiman et al., 2008, 2013; Ralph et al., 2005, 2017). A single AR event can persist through sequential cyclones in favorable atmospheric blocking conditions where a corridor linking the moisture source and sink regions is maintained (Benedict et al., 2019; Sodemann & Stohl, 2013). This results in an AR landfall event sometimes consisting of multiple rounds of heavy precipitation, as mesoscale frontal waves can transport successive vorticity maxima along the edge of a blocking ridge (Dacre et al., 2015; Martin et al., 2019; Neiman et al., 2016). ARs are a crucial component of the global hydrological cycle, accounting for ~90% of the meridional water vapor transport while covering just ~10% of the earth's zonal circumference in the midlatitudes (Nash et al., 2018; Zhu & Newell, 1998).

When ARs approach polar regions, they become very important to snowfall and melt processes in the cryosphere. The enhanced radiative fluxes associated with the anomalously high liquid water content in the clouds contribute to sea ice disintegration in the Arctic (Hegyi & Taylor, 2018; Komatsu et al., 2018), ice mass loss over the Greenland ice sheet (Mattingly et al., 2018; Neff, 2018; Neff et al., 2014), sea ice melt preconditioning for Weddell Sea polynya formation (Francis et al., 2020), and large scale surface melt in West Antarctica (Wille et al., 2019). While ARs can deliver enhanced atmospheric water vapor that increases the chances for surface melt, the anomalously high moisture content can also lead to heavy snowfall events. At Princess Elisabeth Station in East Antarctica, ARs were shown to be responsible for 74%–80% of accumulated snowfall in 2009 and 2011, which were 2 years of unprecedented AR activity in the past 40 years in that region (Gorodetskaya et al., 2014; Wille et al., 2019). Establishing the AR contribution to Antarctic snowfall would improve our understanding of how EPEs impact the Antarctic SMB and how those changes in SMB might impact sea level rise by offsetting dynamic mass loss (Ligtenberg et al., 2013; Rignot et al., 2019). Using an updated version of the AR detection algorithm first presented in Wille et al. (2019), we present the first complete Antarctic-specific AR climatology from 1980 to 2018. Advancements in tracking AR spatial footprints allow for a more in-depth analysis of grid point specific AR frequency, AR trends, AR-related precipitation which were previously difficult to examine when using an algorithm that only returned AR landfall dates in a quadrant-specific analysis like in Wille et al. (2019). The structure of this follows a discussion of AR frequency (Section 3.1), the AR precipitation budget (Section 3.2), AR and snowfall trends (Section 3.3), precipitation and AR interannual variability correlations (Section 3.4), AR blocking behavior (Section 3.5), and AR frequency correlations with SAM (Section 3.6).

2. Data and Methods

2.1. The Atmospheric River Detection Algorithm

The AR detection algorithm utilized in this study is an updated version of the meridional (v) component of integrated vapor transport (IVT) detection algorithm (referred to as vIVT) originally described in Wille et al. (2019). The algorithm running on a 3-h time step identifies grid cells between 37.5°S and 80°S, where vIVT is at or above the 98th percentile of all monthly vIVT values per grid cell from 1980 to 2018. The percentile is derived from 3-hourly vIVT values within the same month throughout the study period. The 98th percentile was found to be qualitatively better for AR detection as it avoids detecting items that lack a clear filament of narrow, yet intense moisture transport extending from the subtropics and midlatitudes and thus not meeting the AR definition. If the algorithm detects a continuous filament of extreme vIVT that extends at least 20° in the meridional direction, it is classified as an AR. Here, vIVT (kg m^{-1} s^{-1}) is calculated as

$$\text{vIVT} = -\frac{1}{g}\int_{\text{surface}}^{\text{top}} qv\,dp, \tag{1}$$

where q (kg kg^{-1}) is the specific humidity, where v is the meridional wind velocity (m s^{-1}), g (m s^{-2}) is the gravitational acceleration, and p is the atmospheric pressure (hPa). The calculation of vIVT incorporates all reanalysis levels.

Wille et al. (2019) developed two detection algorithm schemes based on the 98th percentile of monthly integrated water vapor (IWV) and vIVT. In the aforementioned study, it was demonstrated that IWV was a slightly more appropriate choice for studying the effects of ARs on surface melting as ARs detected with the IWV scheme lasted slightly longer after the landfall time when melting was still ongoing. Excessive IWV over the ice sheet is related with the development of mixed-phase clouds containing anomalously high liquid and ice water paths, thus creating high downward longwave radiation fluxes to the surface (Wille et al., 2019). Conversely, the vIVT-based definition of ARs was found to be more appropriate for studying snowfall patterns, since adding the meridional wind speed component reflects the dynamical processes that lead to precipitation generation. Overall, the authors also found little difference in AR detection frequency between the IWV and vIVT detection schemes. The maximum snowfall intensity within ARs increases more linearly with the AR intensity when AR detections and intensities are based on vIVT compared to IWV (Figure S1).

The latest version of the AR detection algorithm uses the common input IVT data from the Atmospheric River Tracking Method Intercomparison Project (Rutz et al., 2019) to facilitate comparisons between participating methods. This means running the detection algorithm on 3-hourly fields from reanalysis vertically integrated on all levels to create an AR catalog (see Equation 1). Whereas the previous version of the detection algorithm was applied individually to quadrants over Antarctica and only returned a date if an AR landfall was detected, the latest version is now run over the entire Antarctic domain with the ability to return the coordinates of discrete AR shapes even if multiple ARs occur in a single time step. This allows for a more detailed analysis of AR climatology and their local impacts. For a direct comparison to the precipitation data provided by the regional atmospheric model Modèle Atmosphérique Régional (MAR; described in the following section; Section 2.2), we created an AR detection catalog initialized with European Centre for Medium-Range Weather Forecasts (ERA)-5 (Hersbach et al., 2020) reanalysis with 0.25° × 0.25° original spatial resolution (interpolated for this application onto a 1° × 1° horizontal grid). We also compare AR results from the ERA-5 catalog with another AR catalog initialized with the Modern-Era Retrospective analysis for Research and Applications, Version 2 (MERRA-2), which has a 0.5° × 0.625° horizontal resolution (Gelaro et al., 2017). Wille et al. (2019) found that using MERRA-2 for detecting AR frequency gave similar results than when using other reanalysis products such as Japanese 55-year Reanalysis (JRA-55) (Kobayashi et al., 2015), ERA-Interim (Dee et al., 2011), and Climate Forecast System Reanalysis (CFSR) (Saha et al., 2010). That study also showed that a reanalysis with a 1° × 1° horizontal grid is likely of a sufficient resolution for AR detection around Antarctica. The AR results presented in this study are from the ERA-5 AR catalog unless stated otherwise.

2.2. Regional Climate Model

The precipitation (rainfall and snowfall) information was obtained from the Modèle Atmosphérique Régional (MARv3.10.2), a regional climate model (RCM) forced by 6-hourly ERA-5 and run at 35 × 35 km^2 horizontal resolution over the Antarctic domain with a 120-s time step and outputs every 3 h (Agosta, Amory, et al., 2019). MAR represents five water species (specific humidity, cloud droplets, ice crystals, raindrops, and snow particles) whose interactions with the air (e.g., evaporation, sublimation, condensation, etc.) contribute directly to the heat and moisture budget of the atmosphere. For instance, sublimation of airborne snow particles during their advection into the atmosphere was shown to be a significant process controlling surface accumulation (Agosta, Amory, et al., 2019). Due to its polar-oriented physics and higher resolution, MAR improves the representation of the Antarctic boundary layer and its interaction with snowfall compared to the driving reanalysis, as well as interactions with snow-covered surface, whereas large-scale circulation patterns are constrained by the forcing fields leading to similar snow accumulation at the surfaces regardless of the reanalysis used in forcing (Agosta, Amory, et al., 2019). Precipitation simulated by MAR diverges significantly from precipitation simulated in various reanalysis products with MAR having higher accuracy when compared against observations (Agosta, Kittel, et al., 2019). The 35 km horizontal resolution of MAR adequately captures precipitation patterns across the continent but does lose some accuracy around the most complex terrain on the Antarctic Peninsula (Agosta, Amory, et al., 2019).

Evaluation of MAR precipitation over Antarctica was performed using the GLACIOCLIM-SAMBA quality-controlled data set of SMB observations containing 3,043 reliable SMB values averaged over more than 3 years (Favier et al., 2013; Wang et al., 2016) and accumulation estimates from Medley et al. (2014). This sparse data set was divided into 10 sectors, each covering large elevation ranges. This model-observation comparison revealed a good representation of the coast-to-plateau SMB gradients in MAR (see Agosta, Amory, et al., 2019 for detailed methodology). Sublimation of precipitation in atmospheric layers is estimated to be of 360 Gt yr^{-1} in MAR for 2015 (Agosta, Amory, et al., 2019), close to the observation-based estimate of 300 Gt yr^{-1} (Grazioli et al., 2017). Comparing MAR accumulation with reanalysis accumulation and observations, Agosta, Kittel, et al. (2019) show that reanalyzes, including ERA5, likely underestimate sublimation in the surface atmospheric layers.

The AR shapes provided by the algorithm were compared against the MAR precipitation (snowfall and rainfall) to calculate the percentage of total precipitation attributed to ARs. Any precipitation that occurred on a grid cell under the footprint of an AR landfall during and within 24 h after the last AR detection over that grid cell is counted toward the grid cell's total AR precipitation. Counting precipitation on the temporal periphery of AR landfalls is helpful as often precipitation succeeds the AR event (Gorodetskaya et al., 2020), since residual moisture after the AR departs may contribute to lingering precipitation (Wille et al., 2019).

2.3. Blocking Index

To analyze the connection between ARs and atmospheric blocking ridges, we created a blocking index inspired by the results of Scott et al. (2019) and Wille et al. (2019) and are visualized in Figure S2. For each AR shape, a 180° azimuth centered on the mean longitude of the AR is created. In a zonal band from 60° to 75°S within the azimuth, we calculate the maximum and minimum 500 hPa geopotential heights compiled over a 24-h period centered around the AR landfall and compare that to the respective monthly average to get anomaly values. The difference between the maximum and minimum height anomalies becomes the blocking index. To compare the AR blocking indices against non-AR blocking indices around Antarctica, four 180° azimuths are created around Antarctica (0°–180°, 90°–270°, 180°–360°, and 270°–90°). For each time step without an AR detection, the difference between the maximum and minimum 24-h averaged height anomalies for each azimuth within the zonal band from 60° to 75°S is calculated. The azimuth with the greatest difference becomes the blocking index for that non-AR time step. We take the blocking index from the azimuth with the highest value to show that AR landfalls are associated with a much higher amplitude jet pattern compared to non-AR days. Geopotential height is provided by ERA-5 and interpolated to a 1° × 1° horizontal resolution.

3. Results

3.1. Atmospheric River Frequency

Overall, ARs occur relatively rarely around Antarctica. Following the framework established in Rutz et al. (2019), AR frequency defined here refers to the percentage of time a particular location is under the spatial footprint of ARs. Based on the default ERA-5 AR catalog, the annual AR frequency is highest over the Southern Ocean at around 1.2% (or 3.5 days per year) and then decreases progressively from the Antarctic coast (~1.0% or 3 days per year) to the interior (Figure 2). The lowest frequency occurs over interior portions of the eastern Antarctic continent near the Transantarctic Mountains (~0.2% or less than 1 day per year; location names are given in Figure 1). On the Antarctic continent, the Antarctic Peninsula, Dronning Maud Land, and Enderby Land have the highest AR frequency of around 1.0%–1.2%. A noticeable minimum in AR frequency is found over the Ross Sea, where a topographically induced cyclonic eddy generally steers extratropical cyclones toward the Amundsen Sea coast (Baines & Fraedrich, 1989). A similar climatology is found using the AR detection algorithm with MERRA-2 data with a slightly higher AR frequency across the study domain (Figure S3). Since cyclones undergo cyclolysis upon landfall from vorticity compression induced from topography, detecting ARs over the continent becomes more complex, and frequency results have to be taken more cautiously far inland.

Previous global detection algorithms may not extend onto the Antarctic continent but do provide AR detection data over the Southern Ocean. For instance, the CONNected-objECT (CONNECT) and Guan and Waliser algorithms have a similar circumpolar swath of maximum AR frequency around Antarctica (Guan & Waliser, 2015; Sellars et al., 2017; Shearer et al., 2020). However, both also have a lower latitude of maximum AR frequency compared to the results presented here. This is likely a product of the 37.5°–80°S domain used here causing maximum AR frequency to be centered toward the middle latitudes around 60°S. The Guan and Waliser algorithm also has a much higher frequency of AR activity (~6%) in locations where we present a frequency of around 1% (Guan & Waliser, 2015).

Breaking down the annual AR climatology into seasons reveals a greater spatial diversity in AR frequency compared to an annual perspective. Like the general pattern of cyclones, there is a greater frequency of ARs in the winter June, July, August (JJA) compared to the summer (December, January, February (DJF); Figure S4). During DJF, the areas of maximum AR frequency are further offshore, with three local maxima at the northern Antarctic Peninsula, Dronning Maud Land, and Enderby Land, specifically near Neumayer and Syowa stations (Figure S4a). In March, April, May (MAM), AR activity increases relative to summer in the Amundsen-Bellingshausen Sea and Wilkes Land especially near Dumont d'Urville station and Davis station (Figure S4b). The highest AR frequency occurs in JJA, with relatively high AR frequency along most of the Antarctic coastline. The areas with the highest AR frequency include most of the Antarctic Peninsula and Enderby Land (Figure S4c). AR frequency remains high in the spring September, October, November (SON) with regional areas of AR frequency maxima near Davis station and particularly further inland near Neumayer station (Figure S4d).

Given the relationship between ARs and extra-tropical cyclones, the AR frequency patterns around Antarctica look similar to the cyclone density from a cyclone tracking algorithm (Guo et al., 2020; Simmonds et al., 2003; Uotila et al., 2013; Zhang et al., 2019). However, while the highest cyclone density is generally found nearby the Antarctic coast, the highest AR frequency occurs further north in the Southern Ocean. This is expected, as ARs generally occur in a highly amplified jet pattern and are defined by the meridional transport of water vapor that originates further north compared to standard cyclogenesis, which typically occurs in a more zonal jet pattern (Chen et al., 2015; Wille et al., 2019).

3.2. Atmospheric River Precipitation Contribution

3.2.1. Mean Precipitation

Despite the rare occurrence of ARs across Antarctica, they have a disproportionately large impact on precipitation across Antarctica. In regard to annual snowfall accumulation, their impacts are most prominent in East Antarctica. ARs are responsible for 10%–20% of annual snowfall that occurs across a broad swath of East Antarctica, as determined by snowfall that occurs within the footprint of an AR during the 24 h after

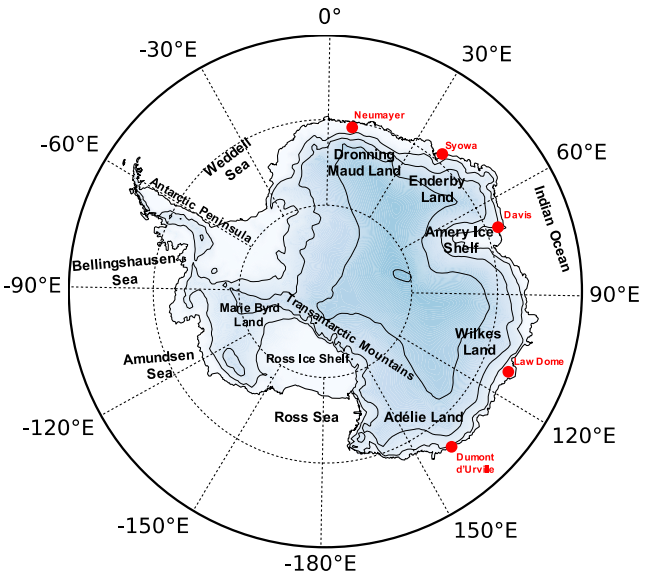

Figure 1. Locations of regions and stations mentioned in the study.

the AR landfall (Figure 3a). The highest percentages (~20%) are found in small pockets across Dronning Maud Land and a region near the southern extent of the Amery Ice Shelf, although the southernmost part of the Amery Ice Shelf receives less snowfall compared to other regions across Antarctica with high AR activity (Figure 3b). Across West Antarctica in Marie Byrd Land, AR activity is less influential with lower percentages (~10%) compared to East Antarctica. This compares relatively similar with the AR precipitation fraction from the global AR detection in Guan and Waliser (2015), although that algorithm has a much high AR frequency with precipitation results only extending to the Antarctic coastline. There is little variation in AR snowfall attribution across the seasons (Figure S5), although there is a noticeable difference in Dronning Maud Land where ARs are most impactful in the summer (DJF; 20%–30%) and have the smallest AR snowfall percentage in fall (MAM, 10%–20%). When comparing snowfall engendered to ARs detected with the ERA-5 catalog and the MERRA-2 catalog, negligible differences appear further bolstering the robustness of the AR detection methodology (Figure S6).

While ARs influence the annual snowfall accumulation more in East Antarctica than in West Antarctica, the opposite is true in regard to the annual rainfall. Along the coastline of the Amundsen and Bellingshausen Seas, where rainfall amounts exceed 5 mm per year, ARs are responsible for ~30% of the total rainfall over several ice shelves along the western Antarctic Peninsula (Figures 3c and 3d). These results are in agreement with the previous rainfall analysis from Wille et al. (2019). As ARs are the primary transport mechanism for heat transport from the tropics and high liquid water content clouds onto the Antarctic continent, it is of little surprise they have a larger fingerprint in rainfall events compared to snowfall events. Yearly rainfall amounts are negligible across most of the remaining Antarctic continent. However, just offshore of the East Antarctic coastline, ARs are responsible for 20%–40% of total rainfall (Figure 3c).

3.2.2. High Precipitation Events

Turner et al. (2019) examined the role of EPEs in precipitation variability across Antarctica and suggested that ARs may represent some of these EPEs. To test how often ARs were responsible for EPEs, we compounded precipitation (snowfall + rainfall) values that were within the 90th, 95th, and 99th percentile of all 3-hourly precipitation from 1980 to 2018. Overlaying these precipitation events with AR occurrence gives insight in the ratio of EPEs explained by ARs. Within all the extreme precipitation event (EPE) percentiles, the precipitation percentage patterns are similar to the snowfall percentages with ARs being responsible for more EPEs in East Antarctica than West Antarctica (Figures 3a and 4). Generally, ARs have a greater impact on the percentage of EPE events in West Antarctica than East Antarctica by about 10 percentage points. Across East Antarctica, the percentage of EPEs attributed to ARs is around 25%–35%, 35%–45%, and 60%–70% when using an EPE threshold of 90, 95, and 99, respectively (Figure 4). This is relatively similar to the AR fraction of EPEs along the Antarctic coastline when using the Guan and Waliser AR detection algorithm (Waliser & Guan, 2017). When we expanded the area of consideration around the AR shapes to take into account precipitation that might fall just outside of the detected AR, we found about a 10 percentage point increase in the AR snowfall fraction for total snowfall and all EPE percentiles (see Section S1 for a full description). Overall, ARs are the source of most EPE events described in Turner et al. (2019) and can quickly significantly alter the mass balance in isolated affected areas on the AIS.

3.3. Atmospheric River and Snowfall Trends

3.3.1. Atmospheric River Frequency Trends

Across most of Antarctica, AR frequency has increased since 1979 as demonstrated in Wille et al. (2019). Here, we show a greater nuance and spatial variability in this result using the ERA-5 AR catalog and corroborating with the MERRA-2 AR catalog. Indeed, from 1980 to 2018, annual AR frequency has increased

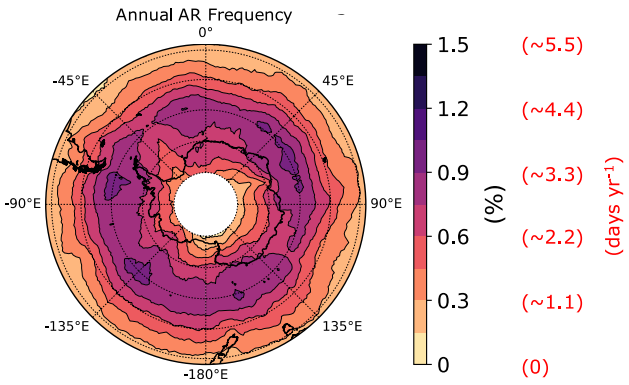

Figure 2. AR frequency (AR days in red) from the vIVT scheme of the AR detection algorithm for 1980–2018. AR, atmospheric river; vIVT, meridional (v) component of integrated vapor transport (IVT).

over more places than decreased across the Southern Ocean and Antarctic continent with the greatest positive trends over the Southern Indian Ocean extending south into Dronning Maud Land and Enderby Land with generally an increase of AR conditions by ~3 h per year (Figure 5b). The only region with a statistically significant decreasing trend in both the ERA-5 and MERRA-2 AR catalogs is Wilkes Land around Law Dome and further inland although at a smaller magnitude (~1.5 h less of AR conditions per year). The trends in the MERRA-2 AR catalog are relatively similar except for a larger increasing trend over West Antarctica and the Amundsen-Bellingshausen Sea, and the lack of a decreasing AR frequency trend along the Amundsen Sea coast (Figure 5a). In Wille et al. (2019), an analysis of AR trends across Antarctica broken into polar stereographic quadrants (Dronning Maud Land and Princess Elisabeth Land, Wilkes Land and Victoria Land, West AIS, Antarctic Peninsula and Weddell Sea region) found similar patterns especially with the increasing annual AR frequency trend on the Dronning Maud Land region (see the supporting information in Wille et al., 2019).

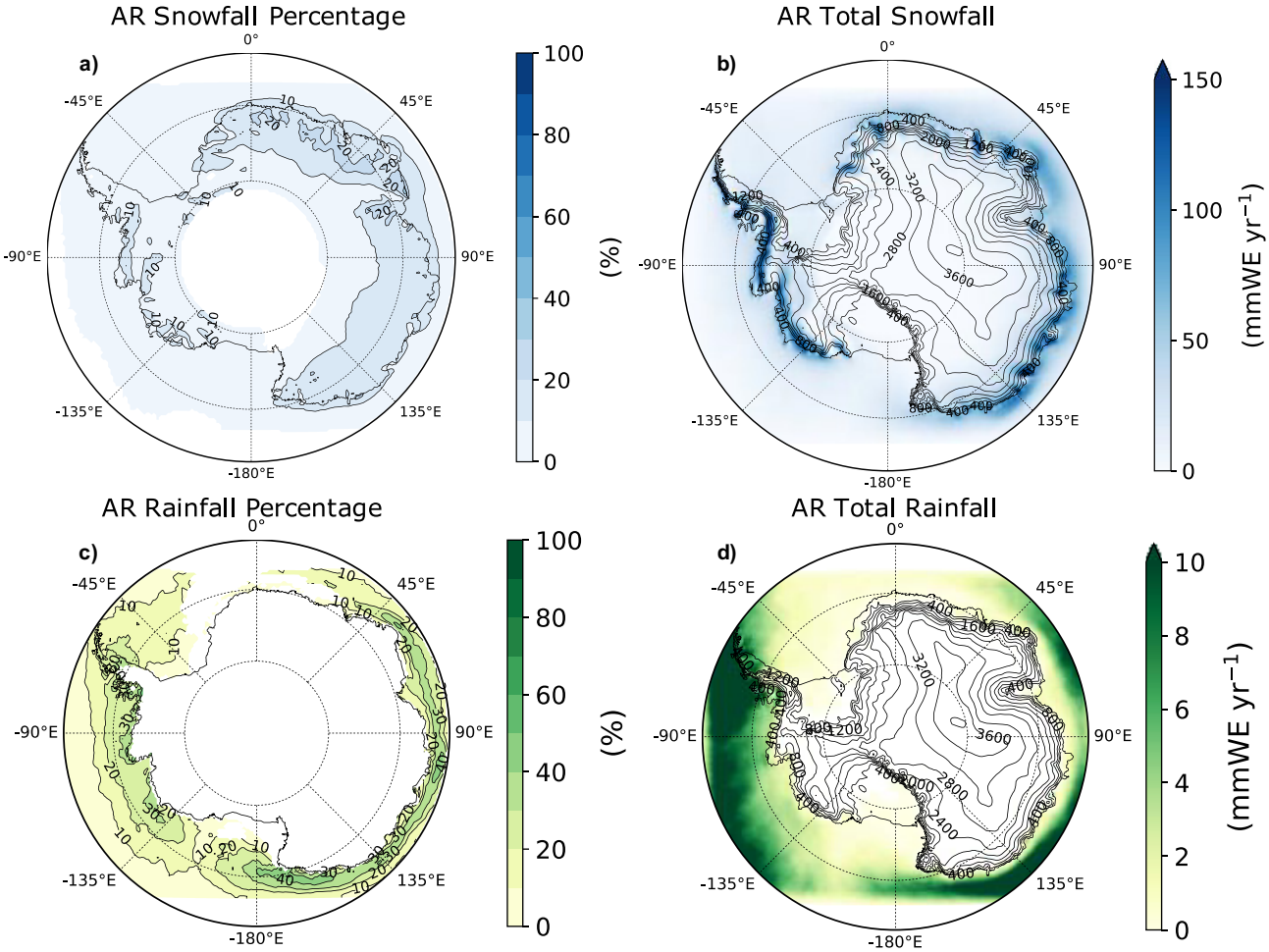

Figure 3. The percentage of the total (a) snowfall and (c) rainfall and the AR-related accumulated (b) snowfall and (d) rainfall simulated by MAR that occurred when an AR made landfall and within 24 h after landfall from 1980–2018. For (c), areas with annual rainfall less than 5 mm per year are not considered. AR, atmospheric river; MAR, Modèle Atmosphérique Régional.

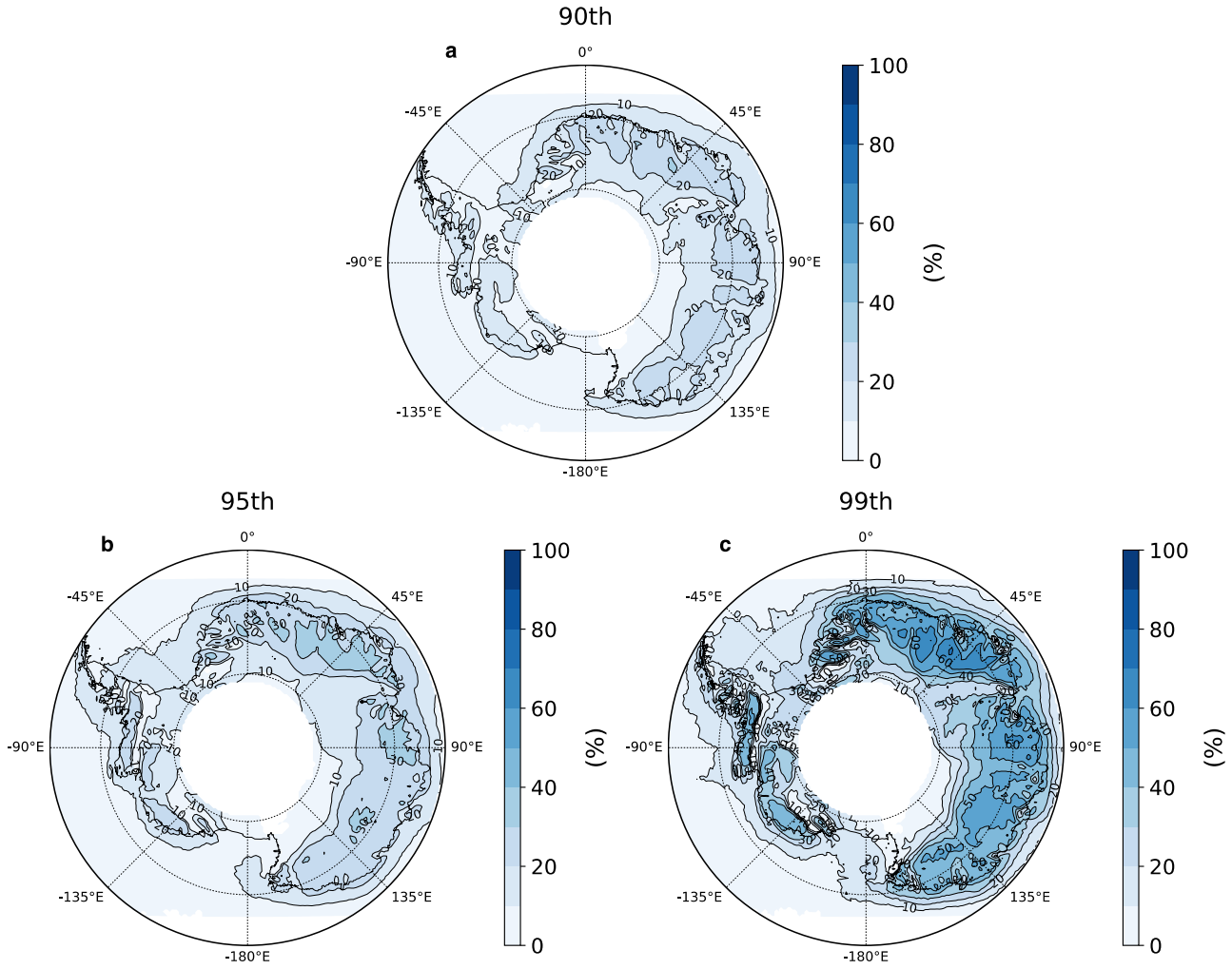

Figure 4. AR extreme precipitation event (EPE) attribution. The percentage of precipitation that occurred when an AR made landfall and within 24 h after landfall when all 3-hourly precipitation weaker than the (a) 90th percentile (b) 95th percentile, and (c) 99th percentile is removed from the precipitation total from 1980 to 2018. AR, atmospheric river.

The AR frequency trends for 1980–2018 become more varied when broken down by seasonality (Figure S8). In Enderby Land, significant positive trends appeared in JJA and SON while further to the west in Dronning Maud Land, the highest positive trends occurred in MAM. Across the Antarctic Peninsula and parts of West Antarctica, significant positive trends were prominent in the shoulder seasons of MAM and SON. Meanwhile along the Amundsen Sea coast/eastern Ross Sea area, relatively large negative trends appear in MAM and JJA.

To further examine the temporal evolution of these trends and put them in the context of previous teleconnection research (e.g., the Interdecadal Pacific oscillation (IPO) reversal in the late 1990s; [England et al., 2014; Vance et al., 2015] and the pause in the SAM trend around 2000 [Banerjee et al., 2020]), we broke down the trends into two periods, 1980–1999 and 2000–2018. In the first half of the reanalysis period (1980–1999), we found a widespread decreasing trend in AR frequency in the Ross Sea and the entirety of East Antarctica of around 1 less AR detection per year (Figures S10a and S10b). Only around Neumayer base (Figure 1), a large positive trend (3–6 h of AR conditions per year) in AR frequency was detected. Since 2000, this general trend reversed, with more regions such as the Ross Sea and especially Dronning Maud Land showing positive trends in AR frequency (3–6 h of AR conditions per year; Figure S10b). In concert with the trend for the entire 1980–2018 period, the greatest negative trend in AR frequency is found in the region surrounding Law Dome in Wilkes Land of around ~5 h less of AR conditions per year. Overall, the

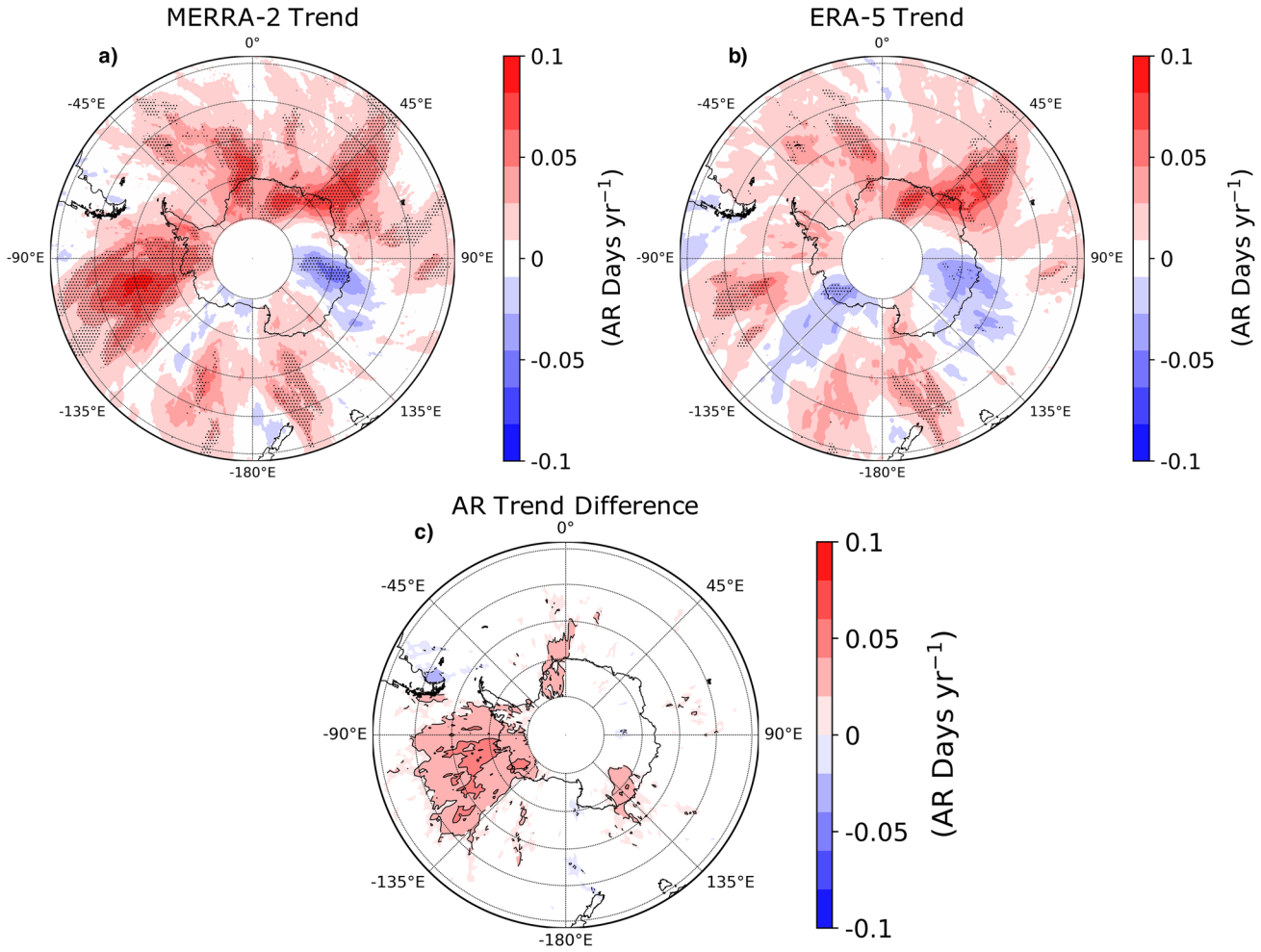

Figure 5. The trends in annual AR frequency measured by detections per year from 1980 to 2018 seen in the AR catalog from (a) MERRA-2, (b) ERA-5, and (c) the difference in trends between the two catalogs. Black circles represent areas of significant trends (p-value < 0.025). AR, atmospheric river; MERRA-2, Modern-Era Retrospective analysis for Research and Applications, Version 2.

negative trend in Wilkes Land appears to have a smaller magnitude in the entire study period 1980–2018, compared to the separate trends from 1980 to 1999 and 2000 to 2018. From looking at individual trends in this region and the results from Wille et al. (2019), this likely resulted from a couple of years of exceptional frequent AR activity in 2001 and 2002 followed by less active years along with a slight shift toward the west in the most significant decreasing trend from 2000 to 2018. Further research is needed to determine if the simulated trends over these relatively short time periods are part of a longer climatological trend or more related to decadal/multidecadal variability in the climate system.

3.3.2. Precipitation Trends

Upon seeing the trends in annual AR frequency, we examine if these trends imprint onto other trends in precipitation across Antarctica. Using MAR rainfall and snowfall data, we show there are noticeable trends in snowfall accumulation across Antarctica, some significant, but no significant trends in rainfall anywhere on the continent. From 1980 to 2018, there have been significant increases in snowfall across portions of the Dronning Maud Land and Enderby Land and the western Antarctic Peninsula (~5 mmWE yr^{-1}; Figure 6b). Meanwhile, annual snowfall decreased significantly slightly inland of the Amundsen Sea coast and coastal parts of Wilkes Land. The standard deviation in annual snowfall accumulation along coastal areas is much larger than the observed trends in annual snowfall indicating a large degree of variability (not shown). When breaking down the study period into two time periods, the same aforementioned significant trends appear for both time periods. However, the snowfall trends in Wilkes Land, Enderby Land, Dronning Maud

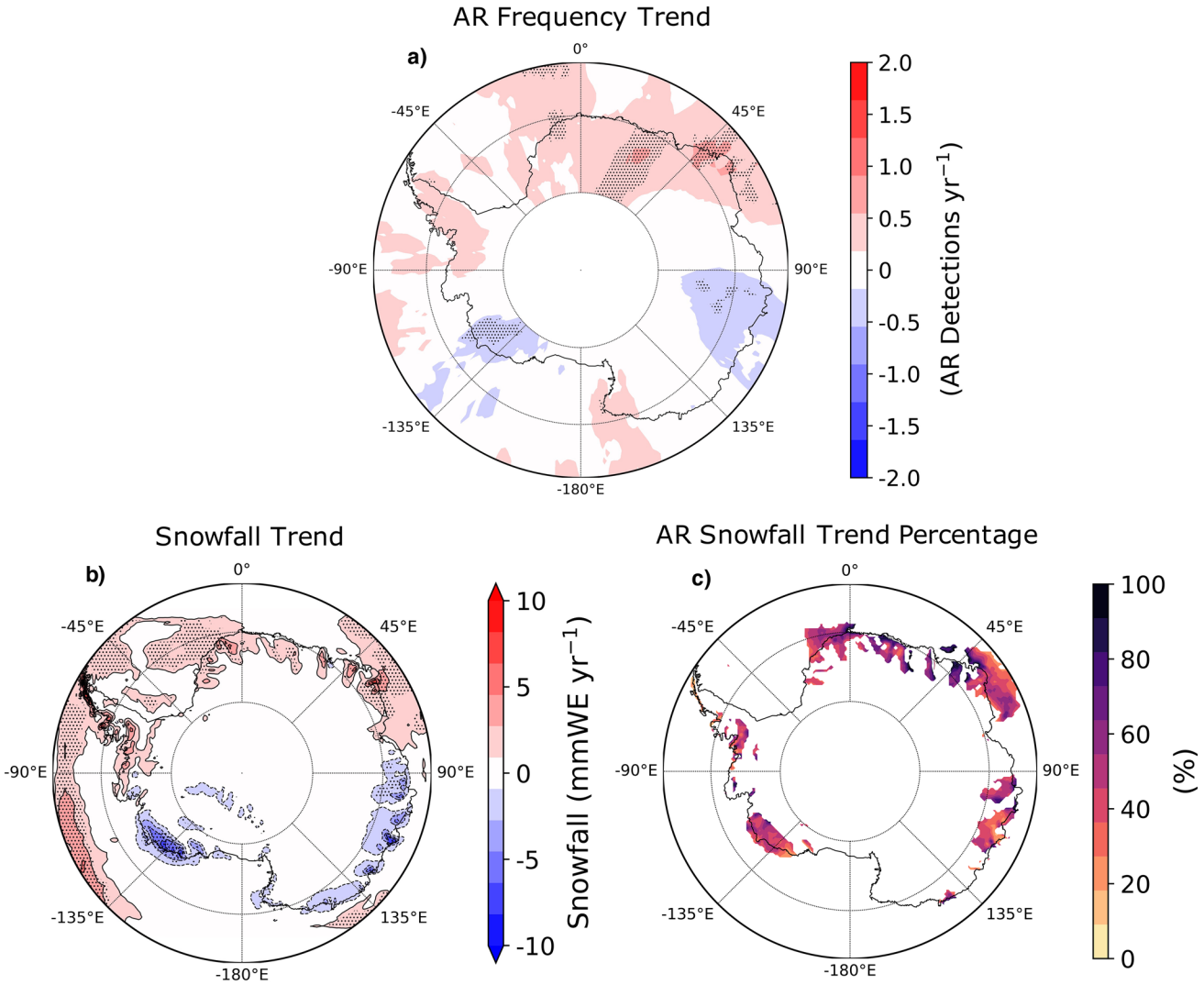

Figure 6. Trends in (a) annual AR frequency, (b) annual snowfall simulated by MAR, and (c) percentage of annual snowfall attributed to AR-related snowfall in areas with absolute snowfall trends greater than 0.5 mmWE yr^{-1} (see Figure 3 for AR-related snowfall totals) from 1980 to 2018. Black circles represent areas of significant trends (p-value < 0.025). AR, atmospheric river; MAR, Modèle Atmosphérique Régional.

Land, and the western Antarctic Peninsula are more amplified for 2000–2018 (Figures S10c and S10d). These trends in the 2000–2018 period in East Antarctica are very similar to the SMB anomalies observed in Regional Atmospheric Climate Model (RACMO2) from 2003 to 2012, especially the negative SMB anomalies in Wilkes Land and the positive SMB anomalies in Dronning Maud Land (Lenaerts et al., 2013). Plus, heavy snowfall accumulation over a large spatial extent like observed during ARs is more likely to result in local SMB increases than light snowfall (Souverijns et al., 2018). The negative snowfall trend in Wilkes Land for 1980–1999 also appears reminiscent of the snowfall trends resolved from ice cores for 1957–2000 (Medley & Thomas, 2019). It is important to note the snowfall trends with regional climate simulations forced by various reanalysis products become more similar after 2000 (Agosta, Amory, et al., 2019).

When comparing trends in annual AR frequency against annual snowfall trends (Figures 6a and 6b), it appears quite clear that the positive trends in annual snowfall in Dronning Maud Land and Enderby Land are mostly driven by the corresponding increase of annual AR frequency in this region, especially when we computed the percentage of the annual snowfall trends explained by annual AR-related snowfall (Figure 6c). The trend in total annual snowfall reaches +7 to +8 mmWE per year with AR-related snowfall accounting for a majority of the trend (Figure 6). Meanwhile, the negative annual snowfall trends in Wilkes

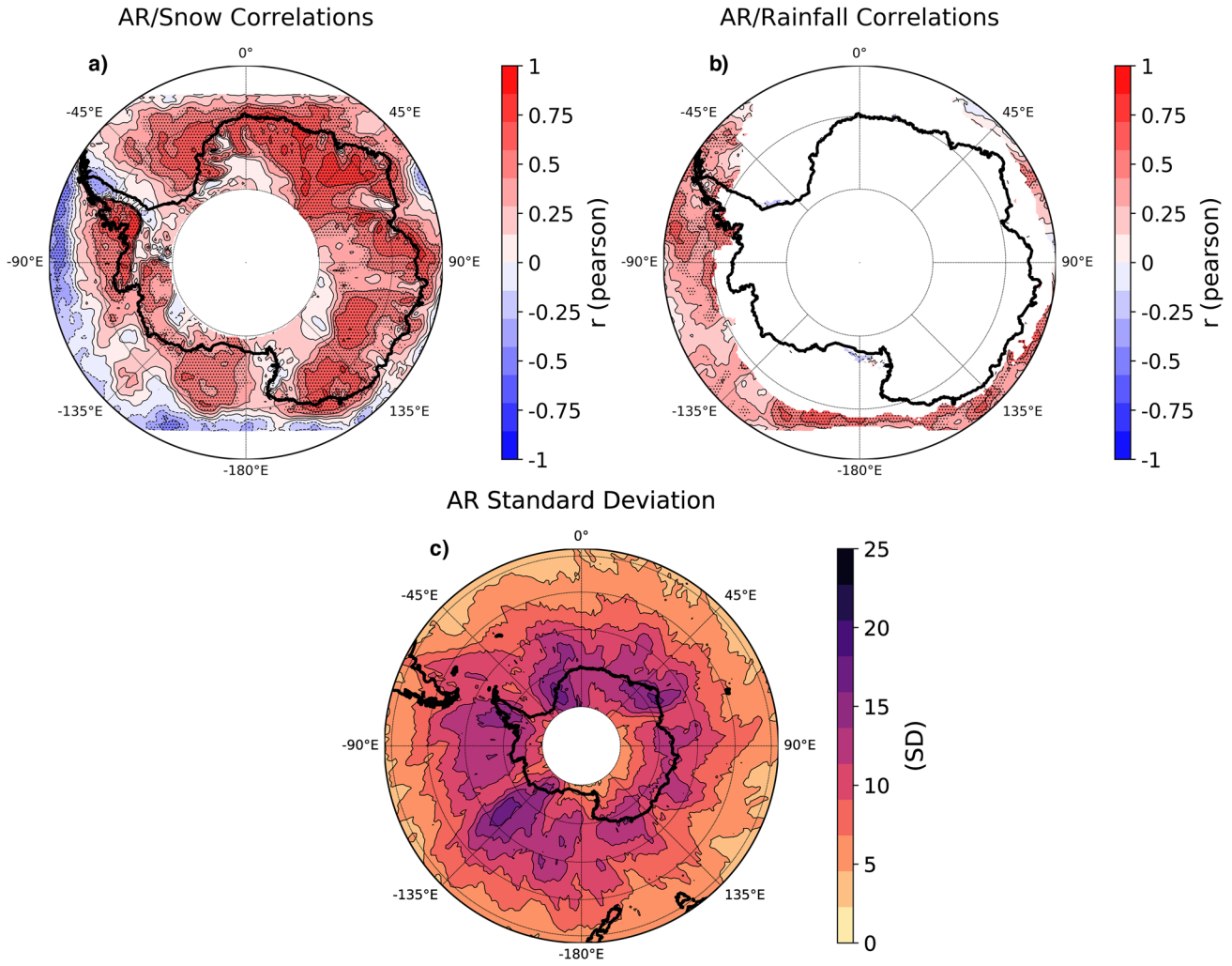

Figure 7. The Pearson's correlation coefficient (*r*-values) between annual AR frequency and (a) total annual snowfall accumulation and (b) total annual rainfall from MAR for 1980–2018. Areas with less than 5 mm of annual rainfall are not considered for (b). Black circles represent areas of significant correlations (p-value < 0.025). (c) The standard deviation in annual 3-hourly AR occurrences from 1980 to 2018. All data sets are detrended and the blank circle in (a) and (b) are regions outside of the AR detection algorithm domain. AR, atmospheric river; MAR, Modèle Atmosphérique Régional.

Land appear partially related to the corresponding decreasing trends in annual AR frequency. Significant negative trends in AR-related snowfall shift slightly west from 1980–1999 to 2000–2018 periods following the pattern in annual AR frequency trends and account for some of the corresponding decreasing trends in annual snowfall (Figure S10). The AR-related snowfall trends along the Amundsen Sea coast are more complicated. As mentioned before, a statistically significant decrease in annual frequency appears in the ERA-5 AR catalog, but not the MERRA-2 catalog. Within the ERA-5 AR catalog, a corresponding decrease in annual AR-related snowfall is evident that explains about 40%–60% of the total annual decrease in snowfall there. These decreases in AR-related snowfall are greatest during MAM and JJA (Figure S9). Elsewhere on a seasonal scale, a large increasing snowfall trend in western Dronning Maud Land during MAM (not shown) appears to be partially driven by a similar trend in AR-related snowfall the same season (Figure S9).

3.4. Atmospheric River Interannual Variability and Precipitation

While a few regions in Antarctica exhibit notable trends in annual AR frequency, Wille et al. (2019) demonstrated a large amount of interannual variability for ARs across most of Antarctica. This is further quantified in this study: The standard deviation of annual AR frequency from 1980 to 2018 is around 20 AR detections (detected at a 3-hourly rate) or about 2.5 days over Enderby and Dronning Maud Land (Figure 7c). The

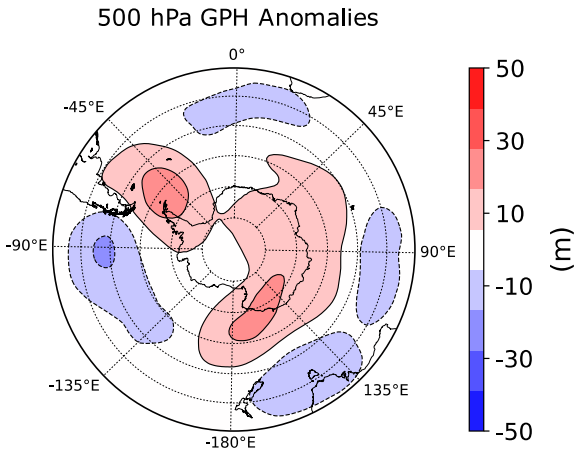

Figure 8. Composite MERRA-2 500 hPa geopotential height anomalies for all AR landfalls from 1980 to 2018. Monthly anomalies are with respect to the corresponding 1980–2018 monthly mean and then averaged together for this annual anomaly. AR, atmospheric river; MERRA-2, Modern-Era Retrospective analysis for Research and Applications, Version 2.

high variability over Enderby Land is the product of unprecedented AR activity in this region during 2009 and 2011 (Gorodetskaya et al., 2014). Around the rest of coastal Antarctica, the standard deviation is around 15 AR detections (~2 days) per year. While there are appreciable trends in annual AR frequency across the continent, the interannual variability in AR frequency is a far more prominent signal.

While ARs appear to control long-term snowfall trends in certain portions of Antarctica, they control the interannual variability of snowfall basically across most of the ice sheet. After removing the trends from both data sets, the annual AR frequency and annual snowfall accumulation across East and parts of West Antarctica are statistically significantly positively correlated from 1980 to 2018 with Pearson correlation coefficients (r) from 0.5 to 0.75 (Figure 7a). On a seasonal scale, the strongest relationship between ARs and snowfall occurs during JJA where nearly most of the Antarctic continent has a significant correlation above 0.5 (Figure S11), but widespread high correlations exist in the other seasons as well. During winter, a significant positive relation appears on the western side of the Antarctic Peninsula (r = 0.5–0.75) while a nonsignificant negative correlation appears on the eastern side (r = 0.25–0.5). This is likely reflective of the fact that most ARs make landfall on the western side of the Peninsula and create a precipitation shadow on the other side of the mountain range. From Wille et al. (2019), we also know that the winter ARs generating snowfall on the western Antarctic Peninsula are also responsible for a majority of the winter surface melting that occurs. There is a negligible difference in the correlation of AR frequency and annual snowfall when comparing the ERA-5 AR catalog against the MERRA-2 AR catalog (not shown).

There are small areas of significant anticorrelations between AR activity and snowfall offshore of the western Antarctic Peninsula in the South Pacific Ocean (Figures 7a and S11). This implies that the prevalence of ARs and the associated warm air advection over the ocean reduces the likelihood of snowfall. When assessing if this connection extends to rainfall, we see that the interannual variability of rainfall (where climatological yearly rainfall values exceed 5 mmWE yr^{-1}) is significantly positively correlated to AR frequency across most of the offshore regions from Wilkes Land extending eastward across the Southern Ocean to the northern Antarctic Peninsula for 1980–2018 (r = 0.5–0.75; Figure 7b).

3.5. Atmospheric Blocking Analysis

We established that ARs have a major impact on the interannual variability and trends of precipitation across Antarctica, so now we look at what controls AR variability across Antarctica. Wille et al. (2019) showed that AR landfalls across Antarctica are accompanied by a blocking ridge upstream of the landfall location, while Turner et al. (2019) described the presence of a blocking high/low surface pressure couplet crucial for EPEs to occur on the Antarctic continent. A composite of the 500 hPa geopotential heights of all AR landfalls in Antarctica from 1980 to 2018 shows a broad area of positive height anomalies over the continent with maxima over the Antarctic Peninsula and Wilkes Land (Figure 8). Meanwhile, areas of negative height anomalies are seen in a circular band from 40° to 50°S. Seasonally, the highest, most widespread positive anomalies associated with AR landfalls occur during MAM while the lowest are in DJF (Figures S12a and S12b). During JJA, three distinct positive anomaly maxima occur around the Antarctic Peninsula, Wilkes Land, and Dronning Maud Laud (Figure S12c). The upper level height patterns suggest that an enhancement of the wavenumber-3 pattern promotes increased AR landfalls in every season with seasonal variations in position (Figure S12a; Cai et al., 1999). Similar 500 hPa geopotential height anomalies are seen when using AR landfall dates from the MERRA-2 AR catalog (not shown).

To better understand atmospheric blocking around Antarctica, we use a blocking index as described in the methodology to quantify the magnitude of blocking associated with AR landfalls. In general, AR landfalls are associated with an atmospheric blocking strength that is generally 30–60 m higher than the background blocking index for all months (Figure 9a). The degree of blocking observed during an AR landfall is highest

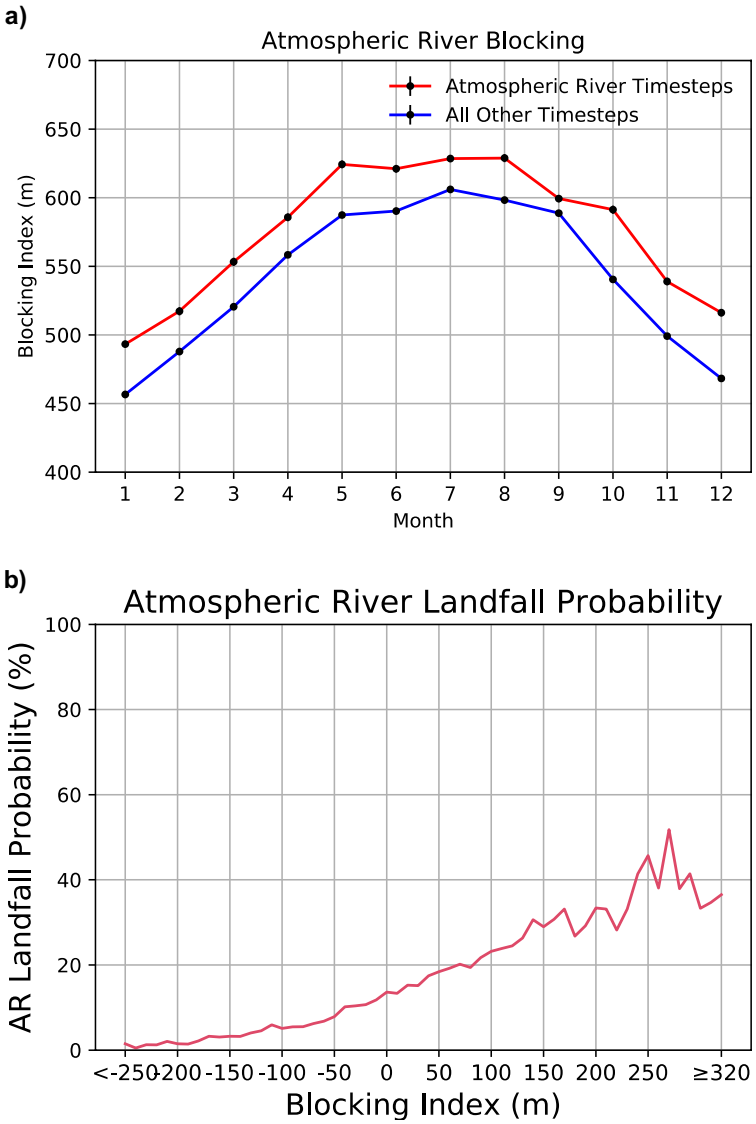

Figure 9. (a) the average monthly blocking index during AR landfalls (red line) and all other time steps (blue line). (b) the probability of an AR landfall in Antarctica based on the value of the blocking index (red line–blue line). The description of the blocking index is found in the Methods (Section 2.3). AR, atmospheric river.

during the winter and lowest during the summer while the background blocking index follows the same pattern. The areas of highest anomalous and lowest anomalous 500 hPA geopotential height during AR landfalls on average occur as couplets along a similar latitude (~63°S, ±0.05°). Typically, these couplets are spaced ~18° ± 0.59° longitude apart from one another. These results imply that relatively tightly packed blocking high-/mid-level low-pressure anomaly couplets that are on a common parallel are most likely to create a corridor for intense moisture transport from the subtropics and midlatitudes to the Antarctic continent.

The difference between the blocking index for AR landfalls and the climatological background could potentially be useful as a predictive index on synoptic timescales. While cyclone activity is an omnipresent occurrence in the Southern Ocean around Antarctica, atmospheric blocking is more likely to create the strong poleward moisture fluxes that are defined as ARs and reach the Antarctic continent as opposed to a more zonal moisture flux (Wille et al., 2019). Compiling the observed blocking index for all AR landfalls against the monthly climatological blocking index shows that the probability of an AR landfall increases as the

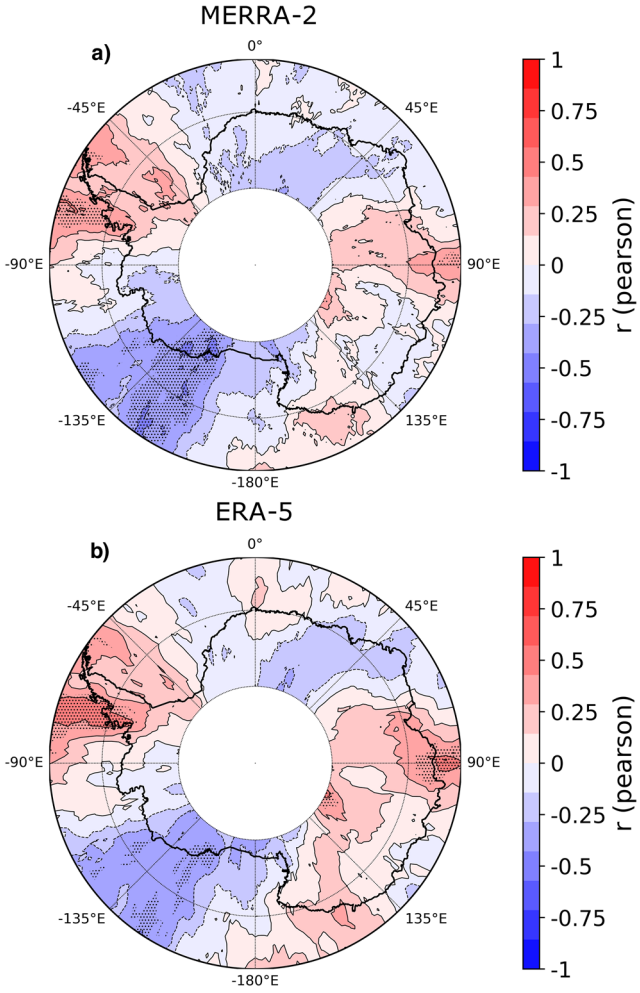

Figure 10. The Pearson's correlation coefficient (*r*-values) between annual AR frequency and annually averaged Marshall SAM index from 1980 to 2018 using (a) the MERRA-2 AR catalog and (b) the ERA-5 AR catalog. Black circles represent areas of significant correlations (p-value < 0.025) and both data sets are detrended. AR, atmospheric river; MERRA-2, Modern-Era Retrospective analysis for Research and Applications, Version 2; SAM, Southern Annular Mode.

blocking index increases (Figure 9b). When the blocking index is greater than 200 m, there is a ~40% probability of an AR landfall in Antarctica. As a potential AR forecast tool over synoptic time-periods, this blocking index analysis would need to be examined over different regions of Antarctica as the probability of an AR landfall is dependent on the latitude of the coastline (Wille et al., 2019).

3.6. ARs and Teleconnections

3.6.1. Correlations to SAM

The Southern Annular Mode (SAM), the leading empirical orthogonal function of geopotential height in the southern hemisphere mid-to-high latitudes, is known to represent opposite pressure fluctuations between Antarctica and the midlatitudes, and thus exerts a physical influence on the Southern Ocean storm tracks (Spensberger et al., 2020; Thompson & Wallace, 2000). The positive polarity of the SAM (SAM+) corresponds to a low pressure over Antarctica and a poleward shift of the midlatitude jet and storm tracks across the Southern Ocean (or, in winter, a local strengthening in the "split jet" region of the Southeast Pacific). Conversely, the negative polarity (SAM−) has high pressure over Antarctica, and the jet shifts equatorward or even disappears in the Pacific in winter (Codron, 2007; Thompson & Wallace, 2000). The zonal distribution of the 500 hPa geopotential height anomalies associated with AR landfalls in Figure 8 resembles the SAM−. Using a detrended Marshall SAM index (Marshall, 2003), we see that AR interannual and SAM interannual variability are significantly correlated in certain areas (Figure 10). From 1980 to 2018, annual AR variability was significantly correlated to SAM on the western Antarctic Peninsula and anticorrelated around the Amundsen-Ross Sea (Figure 10a). The MERRA-2 AR catalog has a slightly weaker yet still significant correlation over the Antarctic Peninsula and a stronger and more significant anticorrelation around the Amundsen-Ross Sea for 1980–2018 (Figure 10b). Seasonally, the strongest anticorrelation with AR variability and SAM in the Amundsen-Ross Sea region occurred during winter (JJA; Figure S13c), while summer (DJF) actually has a significant positive correlation focused over the Amundsen Sea (Figure S13a). The weakest correlations over the Antarctic Peninsula occurred during summer (DJF).

Outside of West Antarctica, a slight significant correlation between AR interannual variability and SAM for 1980–2018 is evident east of the Amery Ice Shelf that is stronger when using the ERA-5 catalog (Figure 10). On seasonal scales, a significant anticorrelation appears during MAM in Dronning Maud Laud and during SON in the western Ross Sea although the latter area also has the lowest AR frequency (Figures 2, S13b, and S13c).

3.6.2. Teleconnection Impacts on ARs

Given the results seen in Figure 10, SAM− (westerly winds expanded toward the equator) is more conducive for ARs to reach Marie Byrd Land while SAM+ (westerly winds contracted toward Antarctica) increases the likelihood of ARs reaching the Peninsula. This pattern of positive annual AR frequency/SAM positive correlation on the Antarctic Peninsula and a negative correlation closer to Marie Byrd Land implies that the strength and orientation of the Amundsen Sea Low (ASL) impacts AR storm tracks. Generally, SAM− is related to a weaker ASL and shifts the ASL southward, a weaker polar jet with more meandering and allows for more atmospheric blocking and moisture intrusions onto the continent (Scott et al., 2019; Turner et al., 2013). However, if the ASL strength is defined using relative central pressure instead of absolute central pressure (Hosking et al., 2013), then the link to SAM diminishes (Donat-Magnin et al., 2020).

SAM+ is associated with enhanced moisture fluxes toward the Antarctic Peninsula accompanied by a more easterly storm track related to the strengthening of the circumpolar westerlies (Lubin et al., 2008; Marshall et al., 2017). The recovery of the ozone hole favors a SAM− pattern during the austral summer and has already stabilized an increasing SAM trend since 2000 which could influence future AR frequency around Western Antarctica given the positive correlation between SAM and annual AR frequency in this region (Figure 10; Banerjee et al., 2020). However, increasing greenhouse gas forcing, which is a year-round forcing, may negate the ozone recovery-induced summer SAM− trend. This makes future SAM trends and associated changes in AR behavior difficult to predict (Gerber & Son, 2014; Wang et al., 2014). While variability in the ASL may explain the AR/SAM correlations in West Antarctica, the positive correlation east of the Amery Ice Shelf is harder to explain and requires further analysis.

Beyond the SAM, the change to a more positive trend from 1980–1999 to 2000–2018 in the Ross Sea matches the trend in increasing blocking activity and surface melting after 2000 as observed in Scott et al. (2019) (Figures S10a and S10b). In addition, the highest increase in seasonal AR frequency is observed during the austral summer months and maybe related with the recent AR-related surface melting events over Marie Byrd Land (Figure S8a; Nicolas et al., 2017; Wille et al., 2019). However, there is not a clear teleconnection explanation for the increase in blocking since 2000 (Scott et al., 2019). Overall, the observed correlations between SAM and AR frequency are preliminary results, and further research is required to properly understand the SAM/AR relationship, plus other teleconnections like the El Niño-Southern Oscillation which may influence the ASL and blocking around West Antarctica (Scott et al., 2019). Idealized model simulations would be an appropriate method for future studies to better understand these processes.

4. Discussion and Conclusions

ARs represent short-term extreme weather events that have significant impacts on the AIS SMB. ARs were previously shown to be associated with around 40% of the surface melt fraction along the Ross Ice Shelf/Marie Byrd Land region (Wille et al., 2019), and as we show here, account for a lower fraction of the overall precipitation across Antarctica, yet engender more absolute snowfall accumulation than surface melt. Due to the short life span and rarity of an AR event (typically affecting coastal regions 3 days per year), their impacts on the SMB are often missed when focusing on changes in the mean climate. By creating a climatology of ARs around Antarctica, we establish their impacts on the trends and variability of precipitation and highlight the external forcings and teleconnections that control AR behavior. Breaking down precipitation components, we show that while ARs contribute a modest percentage (∼20%) of the annual snowfall across the parts of the AIS, they are responsible for a majority of annual snowfall trends across parts of East Antarctica. ARs maybe more influential in East Antarctica due to the generally lower annual snowfall accumulation from less cyclonic activity making near-coastal regions of East Antarctica more sensitive to EPEs which are shown to control the interannual variability of snow accumulation (Hoskins & Hodges, 2005; Turner et al., 2019). We show ARs are connected with EPEs given that 70% of the highest 1% of precipitation events can be attributed to ARs across East Antarctica. ARs are also responsible for ∼30% of rainfall on the coastal regions of the western Antarctic Peninsula. In general, ARs are more influential on snowfall processes in East Antarctica and surface melt processes in West Antarctica but have controlled the interannual variability of precipitation across most of the continent since 1980.

The polarity of the SAM appears related to AR occurrences through the relationship between SAM and the ASL. A positive (negative) SAM phase deepens (weakens) the ASL and shifts its position to direct the storm track toward (away) the Antarctic Peninsula (Amundsen-Ross Sea coast; Turner et al., 2013). Atmospheric blocking serves as the main control mechanism for AR landfalls, and the 500 hPa geopotential height patterns favorable for AR landfalls resemble the SAM− which has been shown to favor blocking patterns over West Antarctica (Scott et al., 2019). However, the higher velocity zonal winds often observed during SAM+ do not preclude a high-amplitude jet-stream and blocking as observed during a series of intense AR landfalls in Marie Byrd Land in January 2016 (Nicolas et al., 2017). Further research is necessary to properly understand how SAM, tropical forcings, and sea surface temperature variations interact to create blocking patterns conducive for AR landfalls, especially in East Antarctica where the AR relationship with SAM appears less clear.

Previous to this study, the only climatology of ARs nearby Antarctica came from a global AR detection algorithm (Guan & Waliser, 2015). The AR frequency as determined by this algorithm generally reaches a maximum in the midlatitudes then decreases poleward and shows a higher frequency of ARs in the Southern Ocean compared to the climatology presented here (Rutz et al., 2019). Regional AR detection algorithms designed for polar regions are advantageous for the higher latitudes as they can account for the reduced moisture capacity of the polar atmosphere (Gorodetskaya et al., 2014; Guan & Waliser, 2015; Mattingly et al., 2018; Wille et al., 2019). As observed in Wille et al. (2019), the choice of reanalysis has little impact on the overall AR detection frequency assuming a reasonable horizontal resolution (~1°). Here, we also observe little difference in results between the AR catalogs forced with ERA-5 and MERRA-2 meaning that our AR detection algorithm is robust and minimally sensitive to the choice of reanalysis. Future work attributing impacts to AR activity should take into account uncertainty in the AR detector and the range of AR frequency from various detection products may affect results (O'Brien et al., 2020).

Using ARs to study moisture transport unites much of the existing literature on "moisture intrusions" in Antarctica into a common framework. ARs are defined by relatively consistent meteorological parameters involving moisture transport mostly embedded within synoptic scale extra-tropical cyclones, so using the AR terminology can make descriptions of moisture intrusions more consistent. The detection algorithm utilized in this study detected ARs that led to high precipitation events in Dronning Maud from 2003 to 2006 (Schlosser et al., 2010), record warmth at Dome Fuji in June 1997 (Hirasawa et al., 2013), the advection of high moisture isotopes into East Antarctica (Kurita et al., 2016; already described as an AR), and record melting and precipitation in Marie Byrd Land (Nicolas et al., 2017; Wille et al., 2019). A more consistent categorization of moisture intrusions has potential benefits for numerical weather prediction as forecasters can look for defined blocking patterns to forecast AR landfalls and their associated impacts on extreme winds, precipitation, and explosive cyclogenesis (Waliser & Guan, 2017; Zhang et al., 2019; Zhu & Newell, 1994). In addition, moisture intrusions and precipitation variability have been shown to impact the interpretation of water stable isotopes and ice core dating (Schlosser et al., 2016; Servettaz et al., 2020; Turner et al., 2019). As ARs are related to many of these events, it is potentially possible to observe an AR impact on past climate reconstructions within ice cores.

A warming climate implies a greater saturation vapor pressure via the Clausius-Clapeyron relationship and thus a greater snowfall potential over the AIS that could offset some sea-level rise from dynamic ice loss (Dalaiden et al., 2020; Ligtenberg et al., 2013; Petit et al., 1999). Understanding atmospheric circulation changes in a moisture atmosphere are essential for future climate projections. Some climate models correctly simulate the present-day atmospheric circulation around Antarctica (Agosta et al., 2015), but we still have limited knowledge on their performance in capturing ARs. Large discrepancies observed in AR detection from National Centers for Environmental Prediction (NCEP)/National Center for Atmospheric Research (NCAR) and DOE need to be fully understood (Wille et al., 2019), and demonstrate that AR retrieval in model simulations is not straightforward. As AR frequency and intensity are predicted to increase in the Southern Ocean in future climate projections (Espinoza et al., 2018), it is paramount for climate simulations to capture changes in extreme weather patterns like ARs to accurately predict the future of the AIS.

Acknowledgments
The authors thank Ambrose Dufour for his assistance in developing the first version of the AR detection algorithm. This study is a part of the PhD project of J. D. Wille conducted at the Université Grenoble Alpes. The authors acknowledge the support from Agence Nationale de la Recherche, projects ANR-20-CE01-0013 (ARCA), ANR-14-CE01-0001 (ASUMA), ANR-16-CE01-0011 (EAIIST), ANR-15-CE01-0005-01 (TROIS AS) and ANR-15-CE01-0015 (AC-AHC2). I. V. Gorodetskaya thanks FCT/MCTES for the financial support to CESAM (UID/AMB/50017/2019), through national funds. C. Agosta acknowledges the support from Fondation Albert 2 de Monaco under the project Antarctic-Snow (2018–2020). J. T. M. Lenaerts was supported by the National Science Foundation under Award No. 1952199. Computational resources have been provided by the Consortium des Équipements de Calcul Intensif (CÉCI), funded by the F.R.S.-FNRS under grant no. 2.5020.11. The manuscript was primarily written in the small village of Stiappa, Tuscany while being graciously hosted by Ugo Nanni.

Data Availability Statement

MERRA-2 vIVT and IWV were compiled and distributed by members of Atmospheric River Tracking Method Intercomparison Project (ARTMIP). The code for the AR detection algorithm discussed in this study is available at https://doi.org/10.5281/zenodo.4009663. The MARv3.10.2 code is available on http://mar.cnrs.fr and the 3-hourly 35 km outputs are available upon request. ERA-5 data produced by ECMWF are available through the Copernicus Climate Data Store. The Marshall Southern Annular Mode (SAM) index is available at https://legacy.bas.ac.uk/met/gjma/sam.html.

References

Agosta, C., Amory, C., Kittel, C., Orsi, A., Favier, V., Gallée, H., et al. (2019). Estimation of the Antarctic surface mass balance using the regional climate model MAR (1979–2015) and identification of dominant processes. *The Cryosphere*, *13*(1), 281–296. https://doi.org/10.5194/tc-13-281-2019

Agosta, C., Fettweis, X., & Datta, R. (2015). Evaluation of the CMIP5 models in the aim of regional modelling of the Antarctic surface mass balance. *The Cryosphere*, *9*(6), 2311–2321. https://doi.org/10.5194/tc-9-2311-2015

Agosta, C., Kittel, C., Amory, C., & Fettweis, X. (2019). Highlights on key polar processes driving the Antarctic surface mass balance. In *Presented at the American Geophysical Union, Fall Meeting 2019 (AGU Fall Meeting 2019)*. San Francisco, CA: Zenodo. https://doi.org/10.5281/ZENODO.4327066

Baines, P. G., & Fraedrich, K. (1989). Topographic effects on the mean tropospheric flow patterns around Antarctica. *Journal of the Atmospheric Sciences*, *46*(22), 3401–3415. https://doi.org/10.1175/1520-0469(1989)046<3401:TEOTMT>2.0.CO;2

Banerjee, A., Fyfe, J. C., Polvani, L. M., Waugh, D., & Chang, K.-L. (2020). A pause in southern hemisphere circulation trends due to the Montreal Protocol. *Nature*, *579*(7800), 544–548. https://doi.org/10.1038/s41586-020-2120-4

Benedict, J. J., Clement, A. C., & Medeiros, B. (2019). Atmospheric blocking and other large-scale precursor patterns of landfalling atmospheric rivers in the North Pacific: A CESM2 study. *Journal of Geophysical Research: Atmospheres*, *124*(21), 11330–11353. https://doi.org/10.1029/2019JD030790

Bozkurt, D., Rondanelli, R., Marín, J. C., & Garreaud, R. (2018). Foehn event triggered by an atmospheric river underlies record-setting temperature along continental Antarctica. *Journal of Geophysical Research: Atmospheres*, *123*(8), 3871–3892. https://doi.org/10.1002/2017JD027796

Bromwich, D. H. (1988). Snowfall in high southern latitudes. *Reviews of Geophysics*, *26*(1), 149. https://doi.org/10.1029/RG026i001p00149

Bromwich, D. H., Guo, Z., Bai, L., & Chen, Q.-s. (2004). Modeled Antarctic precipitation. Part I: Spatial and temporal variability. *Journal of Climate*, *17*(3), 427–447. https://doi.org/10.1175/1520-0442(2004)017<0427:MAPPIS>2.0.CO;2

Cai, W., Baines, P. G., & Gordon, H. B. (1999). Southern mid- to high-latitude variability, a zonal wavenumber-3 pattern, and the Antarctic circumpolar wave in the CSIRO coupled model. *Journal of Climate*, *12*(10), 3087–3104. https://doi.org/10.1175/1520-0442(1999)012<3087:SMTHLV>2.0.CO;2

Chen, G., Lu, J., Burrows, D. A., & Leung, L. R. (2015). Local finite-amplitude wave activity as an objective diagnostic of midlatitude extreme weather. *Geophysical Research Letters*, *42*(24), 10952–10960. https://doi.org/10.1002/2015GL066959

Codron, F. (2007). Relations between annular modes and the mean state: Southern hemisphere winter. *Journal of the Atmospheric Sciences*, *64*(9), 3328–3339. https://doi.org/10.1175/JAS4012.1

Dacre, H. F., Clark, P. A., Martinez-Alvarado, O., Stringer, M. A., & Lavers, D. A. (2015). How do atmospheric rivers form? *Bulletin of the American Meteorological Society*, *96*(8), 1243–1255. https://doi.org/10.1175/BAMS-D-14-00031.1

Dalaiden, Q., Goosse, H., Lenaerts, J. T. M., Cavitte, M. G. P., & Henderson, N. (2020). Future Antarctic snow accumulation trend is dominated by atmospheric synoptic-scale events. *Communications Earth & Environment*, *1*(1), 62. https://doi.org/10.1038/s43247-020-00062-x

Dee, D. P., Uppala, S. M., Simmons, A. J., Berrisford, P., Poli, P., Kobayashi, S., et al. (2011). The ERA-interim reanalysis: Configuration and performance of the data assimilation system. *Quarterly Journal of the Royal Meteorological Society*, *137*(656), 553–597. https://doi.org/10.1002/qj.828

Donat-Magnin, M., Jourdain, N. C., Gallée, H., Amory, C., Kittel, C., Fettweis, X., et al. (2020). Interannual variability of summer surface mass balance and surface melting in the Amundsen sector, West Antarctica. *The Cryosphere*, *14*(1), 229–249. https://doi.org/10.5194/tc-14-229-2020

England, M. H., McGregor, S., Spence, P., Meehl, G. A., Timmermann, A., Cai, W., et al. (2014). Recent intensification of wind-driven circulation in the Pacific and the ongoing warming hiatus. *Nature Climate Change*, *4*(3), 222–227. https://doi.org/10.1038/nclimate2106

Espinoza, V., Waliser, D. E., Guan, B., Lavers, D. A., & Ralph, F. M. (2018). Global analysis of climate change projection effects on atmospheric rivers. *Geophysical Research Letters*, *45*(9), 4299–4308. https://doi.org/10.1029/2017GL076968

Favier, V., Agosta, C., Parouty, S., Durand, G., Delaygue, G., Gallée, H., et al. (2013). An updated and quality controlled surface mass balance dataset for Antarctica. *The Cryosphere*, *7*(2), 583–597. https://doi.org/10.5194/tc-7-583-2013

Francis, D., Mattingly, K. S., Temimi, M., Massom, R., & Heil, P. (2020). On the crucial role of atmospheric rivers in the two major Weddell Polynya events in 1973 and 2017 in Antarctica. *Science Advances*, *6*(46), eabc2695. https://doi.org/10.1126/sciadv.abc2695

Gelaro, R., McCarty, W., Suárez, M. J., Todling, R., Molod, A., Takacs, L., et al. (2017). The modern-era retrospective analysis for research and applications, Version 2 (MERRA-2). *Journal of Climate*, *30*(14), 5419–5454. https://doi.org/10.1175/JCLI-D-16-0758.1

Gerber, E. P., & Son, S.-W. (2014). Quantifying the summertime response of the austral jet stream and Hadley cell to stratospheric ozone and greenhouse gases. *Journal of Climate*, *27*(14), 5538–5559. https://doi.org/10.1175/JCLI-D-13-00539.1

Gorodetskaya, I. V., Kneifel, S., Maahn, M., Van Tricht, K., Thiery, W., Schween, J. H., et al. (2015). Cloud and precipitation properties from ground-based remote-sensing instruments in East Antarctica. *The Cryosphere*, *9*(1), 285–304. https://doi.org/10.5194/tc-9-285-2015

Gorodetskaya, I. V., Silva, T., Schmithüsen, H., & Hirasawa, N. (2020). Atmospheric river signatures in radiosonde profiles and reanalyses at the Dronning Maud Land Coast, East Antarctica. *Advances in Atmospheric Sciences*, *37*(5), 455–476. https://doi.org/10.1007/s00376-020-9221-8

Gorodetskaya, I. V., Tsukernik, M., Claes, K., Ralph, M. F., Neff, W. D., & Van Lipzig, N. P. M. (2014). The role of atmospheric rivers in anomalous snow accumulation in East Antarctica. *Geophysical Research Letters*, *41*(17), 6199–6206. https://doi.org/10.1002/2014GL060881

Gorodetskaya, I. V., Van Lipzig, N. P. M., Van den Broeke, M. R., Mangold, A., Boot, W., & Reijmer, C. H. (2013). Meteorological regimes and accumulation patterns at Utsteinen, Dronning Maud Land, East Antarctica: Analysis of two contrasting years. *Journal of Geophysical Research: Atmospheres*, *118*(4), 1700–1715. https://doi.org/10.1002/jgrd.50177

Grazioli, J., Madeleine, J.-B., Gallée, H., Forbes, R. M., Genthon, C., Krinner, G., & Berne, A. (2017). Katabatic winds diminish precipitation contribution to the Antarctic ice mass balance. *Proceedings of the National Academy of Sciences of the United States of America*. *114*(41) 10858–10863. https://doi.org/10.1073/pnas.1707633114

Grieger, J., Leckebusch, G. C., & Ulbrich, U. (2016). Net precipitation of Antarctica: Thermodynamical and dynamical parts of the climate change signal. *Journal of Climate*, *29*(3), 907–924. https://doi.org/10.1175/JCLI-D-14-00787.1

Guan, B., & Waliser, D. E. (2015). Detection of atmospheric rivers: Evaluation and application of an algorithm for global studies. *Journal of Geophysical Research: Atmospheres*, *120*(24), 12514–12535. https://doi.org/10.1002/2015JD024257

Guo, Y., Shinoda, T., Guan, B., Waliser, D. E., & Chang, E. K. M. (2020). Statistical relationship between atmospheric rivers and extratropical cyclones and anticyclones. *Journal of Climate*, *33*(18), 7817–7834. https://doi.org/10.1175/JCLI-D-19-0126.1

Hegyi, B. M., & Taylor, P. C. (2018). The unprecedented 2016–2017 Arctic Sea ice growth season: The crucial role of atmospheric rivers and longwave fluxes. *Geophysical Research Letters*, *45*(10), 5204–5212. https://doi.org/10.1029/2017GL076717

Hersbach, H., Bell, B., Berrisford, P., Hirahara, S., Horányi, A., Muñoz-Sabater, J., et al. (2020). The ERA5 global reanalysis. *Quarterly Journal of the Royal Meteorological Society*, *146*(730), 1999–2049. https://doi.org/10.1002/qj.3803

Hirasawa, N., Nakamura, H., Motoyama, H., Hayashi, M., & Yamanouchi, T. (2013). The role of synoptic-scale features and advection in prolonged warming and generation of different forms of precipitation at Dome Fuji station, Antarctica, following a prominent blocking event. *Journal of Geophysical Research: Atmospheres*, *118*(13), 6916–6928. https://doi.org/10.1002/jgrd.50532

Hobbs, W. H. (1915). The role of the glacial anticyclone in the air circulation of the globe. *Proceedings of the American Philosophical Society*, *54*(218), 185–225.

Hosking, J. S., Orr, A., Marshall, G. J., Turner, J., & Phillips, T. (2013). The influence of the Amundsen-Bellingshausen Seas low on the climate of west Antarctica and its representation in coupled climate model simulations. *Journal of Climate*, *26*(17), 6633–6648. https://doi.org/10.1175/JCLI-D-12-00813.1

Hoskins, B. J., & Hodges, K. I. (2005). A new perspective on southern hemisphere storm tracks. *Journal of Climate*, *18*(20), 4108–4129. https://doi.org/10.1175/JCLI3570.1

Jullien, N., Vignon, É., Sprenger, M., Aemisegger, F., & Berne, A. (2020). Synoptic conditions and atmospheric moisture pathways associated with virga and precipitation over coastal Adélie Land in Antarctica. *The Cryosphere*, *14*(5), 1685–1702. https://doi.org/10.5194/tc-14-1685-2020

King, J. C., & Turner, J. (2007). *Antarctic meteorology and climatology*. Cambridge University Press.

Kittel, C., Amory, C., Agosta, C., Delhasse, A., Doutreloup, S., Huot, P.-V., et al. (2018). Sensitivity of the current Antarctic surface mass balance to sea surface conditions using MAR. *The Cryosphere*, *12*(12), 3827–3839. https://doi.org/10.5194/tc-12-3827-2018

Kobayashi, S., Ota, Y., Harada, Y., Ebita, A., Moriya, M., Onoda, H., et al. (2015). The JRA-55 reanalysis: General specifications and basic characteristics. *Journal of the Meteorological Society of Japan*, *93*(1), 5–48. https://doi.org/10.2151/jmsj.2015-001

Komatsu, K. K., Alexeev, V. A., Repina, I. A., & Tachibana, Y. (2018). Poleward upgliding Siberian atmospheric rivers over sea ice heat up Arctic upper air. *Scientific Reports*, *8*(1), 2872. https://doi.org/10.1038/s41598-018-21159-6

Kurita, N., Hirasawa, N., Koga, S., Matsushita, J., Steen-Larsen, H. C., Masson-Delmotte, V., & Fujiyoshi, Y. (2016). Influence of large-scale atmospheric circulation on marine air intrusion toward the East Antarctic coast. *Geophysical Research Letters*, *43*(17), 9298–9305. https://doi.org/10.1002/2016GL070246

Lenaerts, J. T. M., van Meijgaard, E., van den Broeke, M. R., Ligtenberg, S. R. M., Horwath, M., & Isaksson, E. (2013). Recent snowfall anomalies in Dronning Maud Land, East Antarctica, in a historical and future climate perspective. *Geophysical Research Letters*, *40*(11), 2684–2688. https://doi.org/10.1002/grl.50559

Ligtenberg, S. R. M., van de Berg, W. J., van den Broeke, M. R., Rae, J. G. L., & van Meijgaard, E. (2013). Future surface mass balance of the Antarctic ice sheet and its influence on sea level change, simulated by a regional atmospheric climate model. *Climate Dynamics*, *41*(3–4), 867–884. https://doi.org/10.1007/s00382-013-1749-1

Lubin, D., Wittenmyer, R. A., Bromwich, D. H., & Marshall, G. J. (2008). Antarctic Peninsula mesoscale cyclone variability and climatic impacts influenced by the SAM. *Geophysical Research Letters*, *35*(2), L02808. https://doi.org/10.1029/2007GL032170

Marshall, G. J. (2003). Trends in the Southern Annular Mode from observations and reanalyses. *Journal of Climate*, *16*(24), 4134–4143. https://doi.org/10.1175/1520-0442(2003)016<4134:TITSAM>2.0.CO;2

Marshall, G. J., Thompson, D. W. J., & van den Broeke, M. R. (2017). The signature of southern hemisphere atmospheric circulation patterns in Antarctic precipitation. *Geophysical Research Letters*, *44*(22), 11580–11589. https://doi.org/10.1002/2017GL075998

Martin, A. C., Ralph, F. M., Wilson, A., DeHaan, L., & Kawzenuk, B. (2019). Rapid cyclogenesis from a mesoscale frontal wave on an atmospheric river: Impacts on forecast skill and predictability during atmospheric river landfall. *Journal of Hydrometeorology*, *20*(9), 1779–1794. https://doi.org/10.1175/JHM-D-18-0239.1

Massom, R. A., Pook, M. J., Comiso, J. C., Adams, N., Turner, J., Lachlan-Cope, T., & Gibson, T. T. (2004). Precipitation over the interior east Antarctic ice sheet related to midlatitude blocking-high activity. *Journal of Climate*, *17*(10), 1914–1928. https://doi.org/10.1175/1520-0442(2004)017<1914:POTIEA>2.0.CO;2

Mattingly, K. S., Mote, T. L., & Fettweis, X. (2018). Atmospheric river impacts on Greenland ice sheet surface mass balance. *Journal of Geophysical Research: Atmospheres*, *123*(16), 8538–8560. https://doi.org/10.1029/2018JD028714

Medley, B., Joughin, I., Smith, B. E., Das, S. B., Steig, E. J., Conway, H., et al. (2014). Constraining the recent mass balance of Pine Island and Thwaites glaciers, West Antarctica, with airborne observations of snow accumulation. *The Cryosphere*, *8*(4), 1375–1392. https://doi.org/10.5194/tc-8-1375-2014

Medley, B., & Thomas, E. R. (2019). Increased snowfall over the Antarctic ice sheet mitigated twentieth-century sea-level rise. *Nature Climate Change*, *9*(1), 34–39. https://doi.org/10.1038/s41558-018-0356-x

Naithani, J., Gallée, H., & Schayes, G. (2002). Marine air intrusion into the Adelie Land sector of East Antarctica: A study using the regional climate model (MAR). *Journal of Geophysical Research*, *107*(D11), ACL6-1–ACL6-16. https://doi.org/10.1029/2000JD000274

Nash, D., Waliser, D., Guan, B., Ye, H., & Ralph, F. M. (2018). The role of atmospheric rivers in extratropical and polar hydroclimate. *Journal of Geophysical Research: Atmospheres*, *123*(13), 6804–6821. https://doi.org/10.1029/2017JD028130

Neff, W. (2018). Atmospheric rivers melt Greenland. *Nature Climate Change*, *8*(10), 857–858. https://doi.org/10.1038/s41558-018-0297-4

Neff, W., Compo, G. P., Martin Ralph, F., & Shupe, M. D. (2014). Continental heat anomalies and the extreme melting of the Greenland ice surface in 2012 and 1889. *Journal of Geophysical Research: Atmospheres*, *119*(11), 6520–6536. https://doi.org/10.1002/2014JD021470

Neiman, P. J., Moore, B. J., White, A. B., Wick, G. A., Aikins, J., Jackson, D. L., et al. (2016). An airborne and ground-based study of a long-lived and intense atmospheric river with mesoscale frontal waves impacting California during CalWater-2014. *Monthly Weather Review*, *144*(3), 1115–1144. https://doi.org/10.1175/MWR-D-15-0319.1

Neiman, P. J., Ralph, F. M., Moore, B. J., Hughes, M., Mahoney, K. M., Cordeira, J. M., & Dettinger, M. D. (2013). The landfall and inland penetration of a flood-producing atmospheric river in Arizona. Part I: Observed synoptic-scale, orographic, and hydrometeorological characteristics. *Journal of Hydrometeorology*, *14*(2), 460–484. https://doi.org/10.1175/JHM-D-12-0101.1

Neiman, P. J., Ralph, F. M., Wick, G. A., Lundquist, J. D., & Dettinger, M. D. (2008). Meteorological characteristics and overland precipitation impacts of atmospheric rivers affecting the west coast of North America based on eight years of SSM/I satellite observations. *Journal of Hydrometeorology*, *9*(1), 22–47. https://doi.org/10.1175/2007JHM855.1

Nicolas, J. P., Vogelmann, A. M., Scott, R. C., Wilson, A. B., Cadeddu, M. P., Bromwich, D. H., et al. (2017). January 2016 extensive summer melt in West Antarctica favoured by strong El Niño. *Nature Communications*, *8*, 15799. https://doi.org/10.1038/ncomms15799

O'Brien, T. A., Risser, M. D., Loring, B., Elbashandy, A. A., Krishnan, H., Johnson, J., et al. (2020). Detection of atmospheric rivers with inline uncertainty quantification: TECA-BARD v1.0.1. *Geoscientific Model Development*, *13*(12), 6131–6148. https://doi.org/10.5194/gmd-13-6131-2020

Petit, J. R., Jouzel, J., Raynaud, D., Barkov, N. I., Barnola, J.-M., Basile, I., et al. (1999). Climate and atmospheric history of the past 420,000 years from the Vostok ice core, Antarctica. *Nature*, *399*(6735), 429–436. https://doi.org/10.1038/20859

Picard, G., Arnaud, L., Caneill, R., Lefebvre, E., & Lamare, M. (2019). Observation of the process of snow accumulation on the Antarctic Plateau by time lapse laser scanning. *The Cryosphere*, *13*(7), 1983–1999. https://doi.org/10.5194/tc-13-1983-2019

Ralph, F. M., Dettinger, M., Lavers, D., Gorodetskaya, I. V., Martin, A., Viale, M., et al. (2017). Atmospheric rivers emerge as a global science and applications focus. *Bulletin of the American Meteorological Society*, *98*(9), 1969–1973. https://doi.org/10.1175/BAMS-D-16-0262.1

Ralph, F. M., Neiman, P. J., & Rotunno, R. (2005). Dropsonde observations in low-level jets over the Northeastern Pacific Ocean from CALJET-1998 and PACJET-2001: Mean vertical-profile and atmospheric-river characteristics. *Monthly Weather Review*, *133*(4), 889–910. https://doi.org/10.1175/MWR2896.1

Rignot, E., Mouginot, J., Scheuchl, B., van den Broeke, M., van Wessem, M. J., & Morlighem, M. (2019). Four decades of Antarctic ice sheet mass balance from 1979–2017. *Proceedings of the National Academy of Sciences of the United States of America*, *116*(4), 1095–1103. https://doi.org/10.1073/pnas.1812883116

Rutz, J. J., Shields, C. A., Lora, J. M., Payne, A. E., Guan, B., Ullrich, P., et al. (2019). The Atmospheric River Tracking Method Intercomparison Project (ARTMIP): Quantifying uncertainties in atmospheric river climatology. *Journal of Geophysical Research: Atmospheres*, *124*(24), 13777–13802. https://doi.org/10.1029/2019JD030936

Saha, S., Moorthi, S., Pan, H.-L., Wu, X., Wang, J., Nadiga, S., et al. (2010). The NCEP climate forecast system reanalysis. *Bulletin of the American Meteorological Society*, *91*(8), 1015–1058. https://doi.org/10.1175/2010BAMS3001.1

Schlosser, E., Manning, K. W., Powers, J. G., Duda, M. G., Birnbaum, G., & Fujita, K. (2010). Characteristics of high-precipitation events in Dronning Maud Land, Antarctica. *Journal of Geophysical Research*, *115*(D14), D14107. https://doi.org/10.1029/2009JD013410

Schlosser, E., Stenni, B., Valt, M., Cagnati, A., Powers, J. G., Manning, K. W., et al. (2016). Precipitation and synoptic regime in two extreme years 2009 and 2010 at Dome C, Antarctica – implications for ice core interpretation. *Atmospheric Chemistry and Physics*, *16*(8), 4757–4770. https://doi.org/10.5194/acp-16-4757-2016

Scott, R. C., Nicolas, J. P., Bromwich, D. H., Norris, J. R., & Lubin, D. (2019). Meteorological drivers and large-scale climate forcing of west Antarctic surface melt. *Journal of Climate*, *32*(3), 665–684. https://doi.org/10.1175/JCLI-D-18-0233.1

Sellars, S. L., Kawzenuk, B., Nguyen, P., Ralph, F. M., & Sorooshian, S. (2017). Genesis, pathways, and terminations of intense global water vapor transport in association with large-scale climate patterns. *Geophysical Research Letters*, *44*(24), 12465–12475. https://doi.org/10.1002/2017GL075495

Servettaz, A. P. M., Orsi, A. J., Curran, M. A. J., Moy, A. D., Landais, A., Agosta, C., et al. (2020). Snowfall and water stable isotope variability in east Antarctica controlled by warm synoptic events. *Journal of Geophysical Research: Atmospheres*, *125*(17), e2020JD032863. https://doi.org/10.1029/2020JD032863

Shearer, E. J., Nguyen, P., Sellars, S. L., Analui, B., Kawzenuk, B., Hsu, K., & Sorooshian, S. (2020). Examination of global midlatitude atmospheric river lifecycles using an object-oriented methodology. *Journal of Geophysical Research: Atmospheres*, *125*(22), e2020JD033425. https://doi.org/10.1029/2020JD033425

Simmonds, I., Keay, K., & Lim, E.-P. (2003). Synoptic activity in the seas around Antarctica. *Monthly Weather Review*, *131*(2), 272–288. https://doi.org/10.1175/1520-0493(2003)131<0272:SAITSA>2.0.CO;2

Sodemann, H., & Stohl, A. (2013). Moisture origin and meridional transport in atmospheric rivers and their association with multiple cyclones. *Monthly Weather Review*, *141*(8), 2850–2868. https://doi.org/10.1175/MWR-D-12-00256.1

Souverijns, N., Gossart, A., Gorodetskaya, I. V., Lhermitte, S., Mangold, A., Laffineur, Q., et al. (2018). How does the ice sheet surface mass balance relate to snowfall? Insights from a ground-based precipitation radar in East Antarctica. *The Cryosphere*, *12*(6), 1987–2003. https://doi.org/10.5194/tc-12-1987-2018

Spensberger, C., Reeder, M. J., Spengler, T., & Patterson, M. (2020). The connection between the southern annular mode and a feature-based perspective on southern hemisphere midlatitude winter variability. *Journal of Climate*, *33*(1), 115–129. https://doi.org/10.1175/JCLI-D-19-0224.1

Stenni, B., Scarchilli, C., Masson-Delmotte, V., Schlosser, E., Ciardini, V., Dreossi, G., et al. (2016). Three-year monitoring of stable isotopes of precipitation at Concordia Station, East Antarctica. *The Cryosphere*, *10*(5), 2415–2428. https://doi.org/10.5194/tc-10-2415-2016

Thompson, D. W. J., & Wallace, J. M. (2000). Annular modes in the extratropical circulation. Part I: Month-to-month variability. *Journal of Climate*, *13*(5), 1000–1016. https://doi.org/10.1175/1520-0442(2000)013<1000:AMITEC>2.0.CO;2

Turner, J., Phillips, T., Hosking, J. S., Marshall, G. J., & Orr, A. (2013). The Amundsen Sea low. *International Journal of Climatology*, *33*(7), 1818–1829. https://doi.org/10.1002/joc.3558

Turner, J., Phillips, T., Thamban, M., Rahaman, W., Marshall, G. J., Wille, J. D., et al. (2019). The dominant role of extreme precipitation events in Antarctic snowfall variability. *Geophysical Research Letters*. *46*, 3502–3511. https://doi.org/10.1029/2018GL081517

Uotila, P., Vihma, T., & Tsukernik, M. (2013). Close interactions between the Antarctic cyclone budget and large-scale atmospheric circulation. *Geophysical Research Letters*, *40*(12), 3237–3241. https://doi.org/10.1002/grl.50560

Vance, T. R., Roberts, J. L., Plummer, C. T., Kiem, A. S., & van Ommen, T. D. (2015). Interdecadal Pacific variability and eastern Australian megadroughts over the last millennium. *Geophysical Research Letters*, *42*(1), 129–137. https://doi.org/10.1002/2014GL062447

Waliser, D., & Guan, B. (2017). Extreme winds and precipitation during landfall of atmospheric rivers. *Nature Geoscience*, *10*(3), 179–183. https://doi.org/10.1038/ngeo2894

Wang, G., Cai, W., & Purich, A. (2014). Trends in Southern Hemisphere wind-driven circulation in CMIP5 models over the 21st century: Ozone recovery versus greenhouse forcing. *Journal of Geophysical Research: Oceans*, *119*(5), 2974–2986. https://doi.org/10.1002/2013JC009589

Wang, Y., Ding, M., van Wessem, J. M., Schlosser, E., Altnau, S., van den Broeke, M. R., et al. (2016). A comparison of Antarctic ice sheet surface mass balance from atmospheric climate models and in situ observations. *Journal of Climate*, *29*(14), 5317–5337. https://doi.org/10.1175/JCLI-D-15-0642.1

Wille, J. D., Favier, V., Dufour, A., Gorodetskaya, I. V., Turner, J., Agosta, C., & Codron, F. (2019). West Antarctic surface melt triggered by atmospheric rivers. *Nature Geoscience*, *12*(11), 911–916. https://doi.org/10.1038/s41561-019-0460-1

Zhang, Z., Ralph, F. M., & Zheng, M. (2019). The relationship between extratropical cyclone strength and atmospheric river intensity and position. *Geophysical Research Letters*, *46*(3), 1814–1823. https://doi.org/10.1029/2018GL079071

Zhu, Y., & Newell, R. E. (1994). Atmospheric rivers and bombs. *Geophysical Research Letters*, *21*(18), 1999–2002. https://doi.org/10.1029/94GL01710

Zhu, Y., & Newell, R. E. (1998). A proposed algorithm for moisture fluxes from atmospheric rivers. *Monthly Weather Review*, *126*(3), 725–735. https://doi.org/10.1175/1520-0493(1998)126<0725:APAFMF>2.0.CO;2

References From the Supporting Information

Houze, R. A. (2014). Clouds and precipitation in extratropical cyclones. In International Geophysics (Vol. 104, pp. 329–367). Elsevier. https://doi.org/10.1016/B978-0-12-374266-7.00011-1

Tsuji, H., & Takayabu, Y. N. (2019). Precipitation enhancement via the interplay between atmospheric rivers and cutoff lows. *Monthly Weather Review*, *147*(7), 2451–2466. https://doi.org/10.1175/MWR-D-18-0358.1